Utrecht University

Master Thesis

Risks associated with hydrogen leakages from existing high-pressure (natural gas) pipelines

Copernicus Institute of Sustainable Development
Utrecht University
University Supervision by Dr. Ir. Hamed Aslannejad
University Second Reader by Dr. Vinzenz Koning
RIVM Supervision by Matthijs de Winter

August 31, 2024

Pieter van Dam - 1087673
MSc Energy Science

Abstract

This study investigates the risks associated with hydrogen transport through high-pressure pipelines, focusing on potential leakages and their impacts. Using Computational Fluid Dynamics (CFD) simulations, various conditions, including soil type, pipe depth, leak size, and groundwater level, were analyzed to understand their influence on hydrogen leakage. A Monte Carlo analysis was employed to account for uncertainties regarding the conditions under which these leakages might occur.

The results indicate that leak size is the most critical factor affecting leakage rates, followed by the type of surrounding soil. The maximum horizontal dispersion of hydrogen was found to be 4.5 meters, suggesting that this should be considered the minimum safety distance to prevent hydrogen-fueled fires. On average, it was determined that approximately 0.06% of the hydrogen transported will leak annually. The environmental impact of these leakages is minimal, particularly when compared to current natural gas emissions. However, the financial implications can be significant, with potential losses accounting for nearly 10% of Gasunie's total profits in the worst-case scenario. These findings underscore the importance of implementing accurate and efficient leak detection methods to mitigate the risks associated with hydrogen transport.

Contents

Acronyms

CFD Computational Fluid Dynamics.

FEM Finite Element Method.

GHG greenhouse gas.

GWP Global Warming Potential.

GWP100 Global Warming Potential over 100 years.

HG Highest Groundwater depth.

LG Lowest groundwater depth.

MG Mean groundwater depth.

NPW Negative Pressure Wave.

P_{95} 95^{th} percentile.

PJ PetaJoule.

PPA Pressure Point Analysis.

RES Renewable Energy Sources.

RTTM Real-Time Transient Modeling.

1 Introduction

1.1 Societal Background

The Netherlands aims to reduce its CO_2 emissions by at least 55% by 2030 compared to 1990 levels (220.5 million tonnes) [1]. To achieve this goal, increasing the use of Renewable Energy Sources (RES) like wind and solar power is crucial. However, there are several challenges with relying more on these renewable sources. One major issue is the intermittency of wind and solar power, due to their dependency on weather conditions to generate power. Moreover, the Dutch electricity grid already faces congestion, making it difficult to add more renewable energy without overloading the system, especially on sunny or windy days [2]. Furthermore, switching heavy industries, such as steel production, to electricity is challenging, highlighting the need for alternative green energy sources [3].

Hydrogen, both as a clean fuel and a clean energy carrier, is considered a crucial component in various energy transition scenarios [4; 5]. It has several applications: it can be used in gas turbines, burners, and internal combustion engines as a fuel [6; 7], and it also serves as a building block for chemical products like synthetic fuels [8; 9]. Additionally, hydrogen can act as an energy carrier that is converted back into electricity using fuel cells [10; 11]. Therefore, green hydrogen emerges as a potential solution to the intermittency of renewable energy sources, grid congestion, and making heavy industry more sustainable. By using renewable electricity to produce green hydrogen, net congestion can be mitigated [12] by generating electricity locally. This approach reduces the need for additional electricity to pass through the already congested grid, instead utilizing the gas infrastructure. Green hydrogen also provides a viable energy source for industries that are difficult to electrify [3]. To meet climate goals and decrease dependency on natural gas, the Dutch government aims to produce 80 PetaJoule (PJ) of green hydrogen and use 100 PJ of hydrogen by 2030 [13].

The planned increase in hydrogen production and usage introduces the need for a safe and reliable hydrogen distribution infrastructure. The Netherlands plans to develop a hydrogen network connecting major industrial regions and harbours to hydrogen production sites and neighboring countries, forming part of the larger European Hydrogen Backbone [14]. A schematic overview of the Dutch hydrogen backbone with relevant city names can be seen in Figure 1.1.

Figure 1.1: A schematic overview of the planned hydrogen backbone in the Netherlands [15]

It is estimated that 85% of the hydrogen network will consist of repurposed natural gas pipelines [16]. Repurposing natural gas pipelines involves replacing valves, thorough cleaning of the pipelines to meet hydrogen purity standards, updating metering equipment, and adopting new methods for pipeline operation and maintenance [16]. These changes are considered minor in cost and workload compared to building new pipelines. Repurposing aligns with the anticipated decline in natural gas demand driven by the phased shutdown of the Groningen gas field by 2024 [17] and the national commitment to energy efficiency and sustainable alternatives. These factors are projected to significantly reduce natural gas transportation, allowing the network's reuse for hydrogen [16]. Repurposing existing pipelines drastically reduces investment costs, as repurposing is four times cheaper than building new pipelines [16].

Despite being cost-effective, repurposing natural gas pipes comes with several challenges. Firstly, hydrogen's lower volumetric energy density, around one-third of natural gas under typical pipeline conditions, necessitates a substantial increase in flow velocity to maintain the same energy output. This increase can lead to accelerated erosion of pipeline walls and components [18]. A second concern is the embrittlement of pipelines. Gas pipelines, predominantly constructed from high-strength steel [19], are susceptible to hydrogen embrittlement, causing earlier failure compared to natural gas [20]. Lastly, due to hydrogen being the smallest molecule, it can penetrate and diffuse through materials more easily, increasing the likelihood of leaks and requiring stricter containment measures [16; 21].

The aforementioned concerns increase the likelihood of hydrogen leakages during transportation. Research is crucial to understanding the environmental, financial, and safety

effects of such leakages. This research seeks to clarify and solve these questions.

1.2 Research Question and Aim

This research aims to integrate the evaluation of hydrogen leakage in underground pipelines, assessing the environmental and financial impact alongside the safety-related risks. It will provide comprehensive insights by identifying the technical and environmental challenges associated with hydrogen leakage. A CFD model is developed to simulate hydrogen leakage from existing natural gas pipelines into the soil, using parameters such as leakage size, flow velocity, soil type, groundwater level, and the depth of the pipeline as model inputs.

This leads to the main research question:

What are the environmental, financial, and safety-related risks of transporting hydrogen through underground natural gas pipelines?

This main research question is further divided into the following sub-questions:

- How much hydrogen leaks from different leak sizes?
- What is the influence of soil type, groundwater level, and depth of the pipe on the leakage rate?
- How much CO_2-eq is emitted due to hydrogen leaks?
- What is the financial impact of hydrogen leaks?
- What is the safety distance required to prevent hydrogen-fueled fires?
- How do parameters such as number of leaks and detection time affect the financial and environmental impact?
- Which leakage detection methods are currently known?

1.3 Scope

This study is specifically focused on hydrogen leakage within the high-pressure transmission network, often referred to as the hydrogen backbone. This network is responsible for transporting hydrogen over long distances and connecting production sites to major industrial users and distribution hubs. It is important to note that this research does not address the hydrogen distribution network or other components of the hydrogen supply chain, such as storage, end-use, or production. Consequently, the findings related to environmental impact, financial risks, and safety concerns are confined to this segment of the hydrogen infrastructure.

2 Theoretical Background

2.1 Pipe Characteristics

The high-pressure pipelines in the Netherlands that are being repurposed for hydrogen transport are primarily constructed from high-strength steel, with wall thicknesses ranging between 11 and 19 mm [16]. These specifications vary depending on the pipeline's diameter and the pressure requirements needed to ensure safe transport. The pipelines are designed to handle operational pressures of up to 50 bar, and there are plans to upgrade certain sections to handle pressures as high as 66 bar [16]. The expected lifespan of these pipelines, after repurposing for hydrogen, is estimated to match or even exceed the original design life for natural gas (40 to 50 years), provided that appropriate maintenance and monitoring are conducted regularly [16]. On average, these pipelines are placed at a depth of 1.75 meters [22]. However, the installation depth can vary depending on the terrain, construction methods, and safety regulations. There is a lawful minimum depth requirement of 1 meter to ensure the pipelines are adequately protected and to minimize the risk of damage from surface activities or natural events [22].

2.2 Transport Characteristics

The working principles of the pipelines play a large role in hydrogen leakage from a pipeline. For example, if the pressure in the pipeline increases the hydrogen will also leak faster [23]. In the Netherlands, the largest part of the high-pressure pipelines that will be freed up for hydrogen transport will have a diameter of 0.91 meter or more. The initial maximum pipe pressure is 50 bar, which could be increased to 66 bar if necessary [16].

According to Huinen [24], the wall thicknesses, pipe diameter, design pressures, and steel qualities currently used in high-pressure natural gas pipelines, are suitable to transport hydrogen under the designed pressures. Even the increase in flow speed due to the lower volumetric energy density, does not form a safety issue [16; 24].

In the early years of hydrogen adaptation (2020-2030), there is a probability that a blend of natural gas and hydrogen will be used. However, since the Dutch natural gas transmission network is made up of various parallel pipelines, Gasunie can free up transmission pipelines for transporting pure hydrogen [16]. In addition to this, according to Wang et al. [14] all TSOs, including Gasunie, are aiming to transport pure hydrogen.

After examining the transport characteristics of hydrogen through pipelines, it should be considered what happens to the hydrogen in case of a leakage. Two factors that could be important are the soil type and groundwater level surrounding the hydrogen backbone since different types of saturated or unsaturated soil have different diffusion and permeability characteristics. Figure 2.1 shows a schematic overview of the influence of the permeability and groundwater level on the flow rate. If the soil has a lower permeability, there are fewer air pockets for the hydrogen to move through, creating more resistance

and a lower flow rate. If the soil is saturated the air pockets are filled with water, which has a higher resistance than air, thus creating more resistance and a lower flow rate.

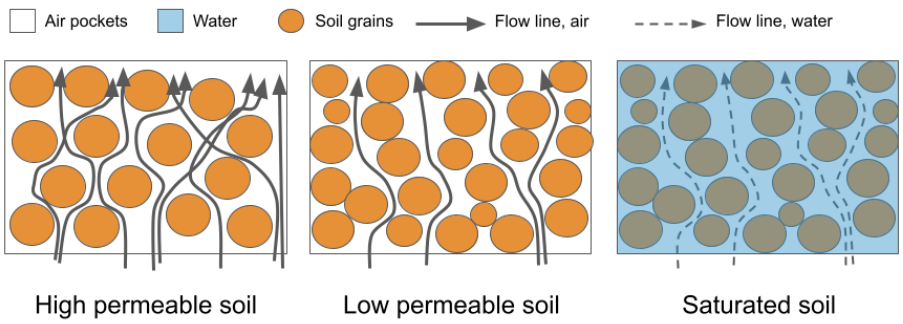

Figure 2.1: A schematic overview of the influence of the permeability of different soil types and the groundwater level on the flow conditions

2.3 Hydrogen Backbone Environment

The first step involves collecting data on the different types of soils and groundwater levels in the Netherlands, particularly near the hydrogen backbone. This data is accessible through dinoloket.nl, which provides comprehensive geoscientific data via the DINO database managed by TNO Geological Survey of the Netherlands (GDN). In Figure 2.2 an example of the data, showing the Lowest groundwater depth (LG), is shown [25]. The groundwater level refers to the level below which the ground is fully saturated with water. The LG is the expected value of the LG3, which is the average of the three lowest groundwater levels recorded in a hydrological year.

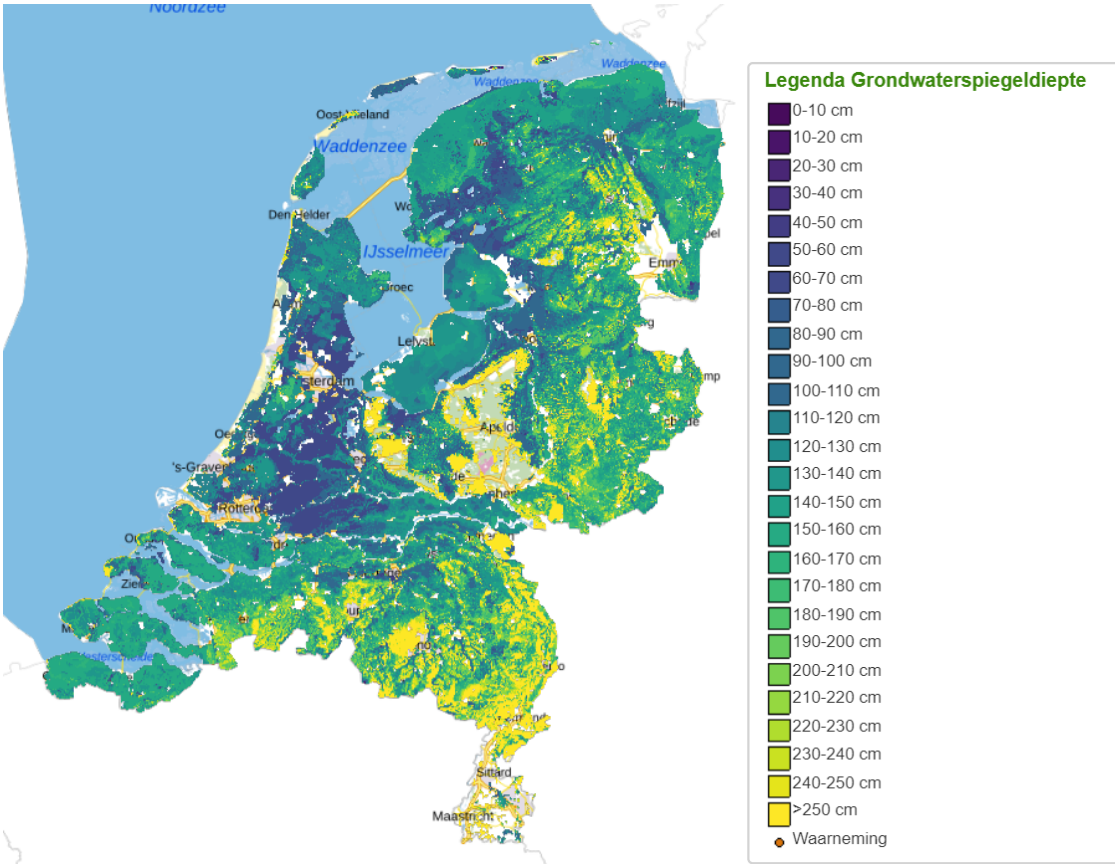

Figure 2.2: The LG in the Netherlands including a legend [25]

2.4 Hydrogen - Soil Interaction

Microbial hydrogen consumption could potentially play a role in the context of hydrogen leakages from underground pipelines, influencing the amount of hydrogen that ultimately reaches the atmosphere. The main processes involved in microbial hydrogen consumption are hydrogenotrophic methanogenesis, acetogenesis, sulfate reduction, and denitrification [26].

Hydrogenotrophic Methanogenesis

Methanogens utilize hydrogen (H_2) to reduce carbon dioxide (CO_2) to methane (CH_4). This process is mainly relevant in conditions without oxygen (anaerobic), such as underground pipelines. A practical example of this process can be observed in biogas production, where organic matter breaks down anaerobically, and methanogens produce methane, which can be used as a renewable energy source. The chemical equation for this process is:

$$4H_2 + CO_2 \rightarrow CH_4 + 2H_2O \tag{2.1}$$

By converting hydrogen into methane, methanogens effectively reduce the amount of

hydrogen that escapes into the atmosphere. This conversion mitigates potential environmental impacts associated with hydrogen leaks [27; 26]. The time span in which this conversion takes place varies significantly depending on factors such as temperature, hydrogen availability, and microbial community composition [28].

Acetogenesis
Acetogens convert hydrogen and carbon dioxide into acetate, which links hydrogen production with methanogenesis and is important in anaerobic conditions. This process is similar to what occurs in the human gut, where acetogenic bacteria help break down dietary fibres, producing acetate as a byproduct, which the body can then absorb as energy. The chemical reaction is:

$$4H_2 + 2CO_2 \rightarrow CH_3COOH + 2H_2O \tag{2.2}$$

Acetogenesis contributes to the reduction of free hydrogen in the soil, thus limiting its release into the atmosphere [29; 30].

Sulfate Reduction
Sulfate-reducing bacteria (SRB) use hydrogen to reduce sulfate (SO_4^{2-}) to sulfide (H_2S). This reaction is analogous to the process that causes the blackening of eggs when boiled for too long, where sulfur in the egg reacts with iron to produce iron sulfide. Sulfate reduction is crucial in anaerobic environments, as shown by the equation:

$$4H_2 + SO_4^{2-} + H^+ \rightarrow H_2S + 4H_2O \tag{2.3}$$

Sulfate reduction is another pathway through which hydrogen is consumed in the soil, preventing its escape into the atmosphere [26; 31].

Denitrification
Denitrifying bacteria reduce nitrate (NO_3^-) to nitrogen gas (N_2) using hydrogen. A common example of this reaction occurs in wastewater treatment plants, where denitrification helps remove excess nitrates, thus preventing water pollution and contributing to the safe release of treated water. The chemical reaction is:

$$4H_2 + 2NO_3^- \rightarrow N_2 + 4H_2O \tag{2.4}$$

This process removes excess nitrogen and also aids in the consumption of hydrogen, limiting its atmospheric release [32].

Syntrophic Interactions
The efficiency of hydrogen consumption in the soil increases through syntrophic (a specific kind of symbiosis) interactions between hydrogen-producing and hydrogen-consuming microorganisms. These interactions, similar to cooperative microbial processes seen in composting, enable microorganisms to exchange important chemicals such as hydrogen and formate, along with organic, sulfurous, and nitrogenous compounds. This collaborative microbial activity significantly mitigates the likelihood of hydrogen escaping into the atmosphere, thereby reducing its potential environmental impact [29; 26].

Implications for Hydrogen Leakages
As shown, microbial hydrogen consumption can play an important role in interacting with hydrogen thus influencing its environmental impact. However, in the context of hydrogen leakages from underground pipelines in this research, this is left out of scope due to the following reasons: the microbial hydrogen uptake is estimated to be insignificant compared to the amount of hydrogen leaked and the large variety in microbial activity dependent on the location and weather conditions [28]. Therefore, this is left out of scope.

2.5 Environmental Impact Hydrogen

Hydrogen is considered an indirect greenhouse gas. In itself, it is not a greenhouse gas but it impacts greenhouse gases such as methane, stratospheric water vapour, ozone as well as aerosols [33]. However, due to the complexity of these reactions and their interaction with each other, there is no consensus yet about the exact impact of hydrogen on the environment.

Hydrogen in the troposphere reacts with OH (hydroxyl radical) [34]. OH is an important oxidant molecule in the atmosphere. Nobel Prize winner Paul Crutzen even named it "detergent of the atmosphere" to describe the crucial cleansing role it plays. OH is created through the following reactions [35]

$$O_3 + UV_{light} \rightarrow O_2 + O \tag{2.5}$$

Then the oxygen atom reacts with water vapour and produces two OH radicals

$$O + H_2O \rightarrow 2OH \tag{2.6}$$

This is why a small amount of ozone is imperative in the troposphere because ozone is the source of OH radicals. Since the first reaction to create OH is created by UV, the OH concentrations show day/night and seasonal cycles. Due to the water vapour that is needed in the second reaction, the concentration of OH decreases with an increase in altitude. The exact concentrations of OH in the atmosphere are hard to measure due to OH's short lifetime of about a second.

OH is the main sink of greenhouse gas (GHG) such as methane (CH_4). It reacts with CH_4 in the following way:

$$CH_4 + OH \rightarrow H_2O + CH_3 \tag{2.7}$$

The methyl radical (CH3) then reacts with oxygen atoms [36]:

$$CH_3 + O_2 \rightarrow CH_3O_2 \tag{2.8}$$

The reaction with OH removes around 92% of the total CH_4 in the atmosphere [37]. However, as stated above OH also reacts with hydrogen. Both reactions can be seen below:

$$H_2 + OH \rightarrow H_2O + H \tag{2.9}$$

$$CH_4 + OH \rightarrow CH_3 + H_2O \tag{2.10}$$

This indicates that when there is more hydrogen in the troposphere, there will be less OH available for methane to react with which will increase the atmospheric lifetime of methane [38; 39; 40; 41; 42].

Both reactions with OH can lead to a generation of ozone in the troposphere by following the radical chain reactions given:

$$H + O_2 \rightarrow HO_2 \tag{2.11}$$

$$HO_2 + NO \rightarrow NO_2 + OH \tag{2.12}$$

$$NO_2 + hv \rightarrow NO + O \tag{2.13}$$

$$O + O_2 \rightarrow O_3 \tag{2.14}$$

this generation of ozone in the troposphere impacts both the air quality and the climate [43; 40]. The reactions of methane and hydrogen also lead to an increase in stratospheric water vapour. This increase in water vapour will increase the infrared radiative capability of the stratosphere. This will lead to the stratosphere cooling as more energy will be lost to space and the overall warming of the climate [44]. An overview of these implications can be found in Figure 2.3.

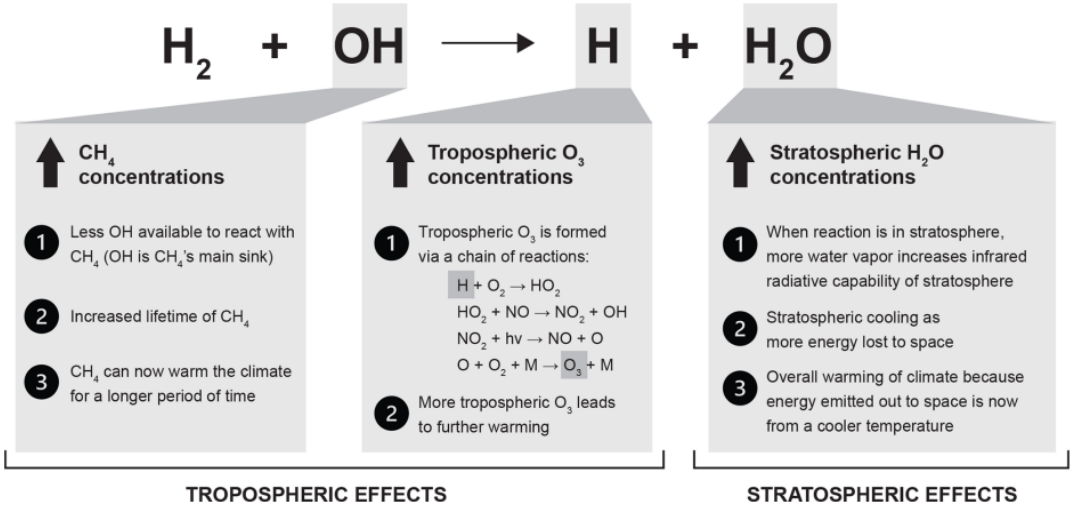

Figure 2.3: Effects of hydrogen on the atmospheric GHG concentrations and warming [44]

However recently Lakshmanan and Bhati [34] found that hydrogen can also react with ozone in the troposphere. This will reduce the amount of ozone in the troposphere (which is considered a positive effect) and there will be more OH available to react with methane. The reaction of hydrogen with ozone is as follows:

$$H_2 + O_3 \rightarrow H_2O + O_2 \tag{2.15}$$

The products of water and oxygen both have no environmental impact in the troposphere. They found that the reaction of H_2 with ozone is thermodynamically favoured over the reaction with OH.

The most common method of quantifying the effect on the environment is the Global Warming Potential over 100 years (GWP100). This is a measure of how much radiative forcing something causes compared to carbon dioxide over 100 years [45]. A higher GWP100 thus indicates a larger potential impact on the environment.

There has been a lot of research regarding the GWP100 of hydrogen, however, the results vary. Sand et al. [33] found that hydrogen has a GWP100 of 11.6 $\pm$ 2.8 (one standard deviation). This GWP100 is more than twice as big as the GWP100 found by Derwent et al. [39], which was equal to 5 $\pm$ 1. Derwent [46] found a GWP100 of 4.3 with a 95 % confidence range from 0 - 9.8. This means if we assume a GWP100 of 11.6, that each kg of hydrogen emitted, is equal to 11.6 kg CO_2-eq. To compare this, one of the main drivers of the heating of the earth, methane, has a GWP100 of 28 - 36 [47].

However recent research by Ocko and Hamburg [44] suggests that hydrogen's impact on the environment is even higher. Ocko and Hamburg [44] states that the impact of hydrogen on the atmospheric warming effect is widely underestimated and overlooked.

This happens because hydrogen has an atmospheric lifespan of two to seven years [48; 46]. However, standard methods to characterize the climate impact usually focus on the long-term impact caused by single bursts of emissions. For gases like hydrogen, with a relatively short lifespan, the long-term impact calculations masks that hydrogen may cause a lot more warming in the short to medium term. Ocko and Hamburg [44] researched this Global Warming Potential (GWP) behavior and the difference between a pulse emission or a constant emission rate as a function of time. The results can be seen in Figure 2.4, which shows that the GWP of hydrogen is much higher in the first few decades compared to 100 years. Ocko and Hamburg [44] found that the GWP100 of the constant emission scenario is approximately 50% higher than the GWP100 (11) of the pulse of emissions. The observed decrease in the GWP of hydrogen over time, even with constant emissions, is attributed to its short-lived indirect warming effects. Hydrogen increases methane's atmospheric lifetime by reducing hydroxyl radical (OH) concentrations, leading to a more significant warming impact in the near term. However, as hydrogen is gradually removed from the atmosphere, its indirect effects on methane and ozone diminish. In contrast, carbon dioxide continues to accumulate, exerting a sustained warming effect [33].

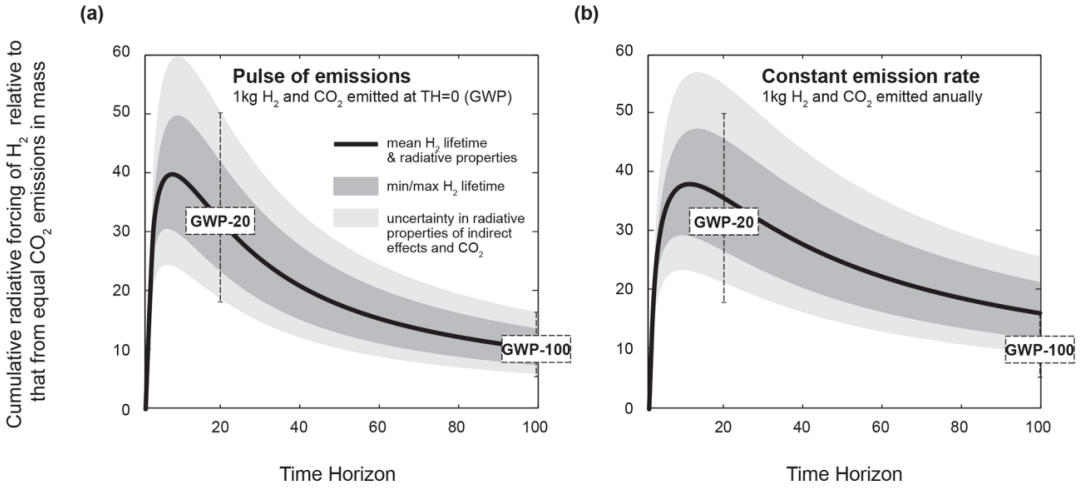

Figure 2.4: The GWP of hydrogen as a function of time. a) there is a one-time pulse of hydrogen, b) there is a constant emission rate of hydrogen. The solid lines depict the average hydrogen lifetime and its radiative impacts, while the darker shaded regions denote the range of hydrogen lifetime considering uncertainty in soil sink estimates. Lighter shaded areas indicate a 20% uncertainty in the radiative effects of hydrogen, considering both its indirect effects and uncertainties in carbon dioxide's radiative properties.

This shows that the climate effects of utilizing hydrogen on a large scale compared to fossil fuels strongly depend on the amount of hydrogen that leaks into the environment during creation, transportation, and utilization. This is also the case for green hydrogen. A possible high emission case in which 10% of the hydrogen production is emitted into the environment shows a reduction of climate impact of only 50% when comparing green

hydrogen and fossil fuels over the first two decades. Over a 100-year time frame, however, climate impacts could be reduced by approximately 80%. In the low emission case where 1% of the hydrogen production is emitted into the environment, there could be an almost 100
% reduction in climate impact compared to fossil fuels [44]. This shows the impact of leakages of hydrogen on the environment and challenges the common perception of green hydrogen energy systems as being completely climate neutral.

To assess the environmental impacts of hydrogen leakages, this study uses the GWP100 metric, which is the most widely accepted measure for determining the climate impact of a gas. Specifically, the GWP100 value for constant emissions found by [44] of 16.5 was used. The constant emissions scenario is similar to the situation considered in this research, leakages that occur throughout the year resulting in a "steady" release of hydrogen.

2.6 Overview of Existing Hydrogen Leakage Models

Models of hydrogen leakages in pipes already exist. Zhang and Zhao [23] found that soil corrosion and hydrogen embrittlement are the main factors behind hydrogen pipeline failure. They found that as the hydrogen pipeline experiences leaks, the concentration of hydrogen in the soil above the leak rises proportionally to the duration of the leakage, following a symmetrical distribution pattern. Moreover, as pipeline pressure rises, the rate of hydrogen leakage accelerates, with longitudinal diffusion gradually becoming the dominant direction. Additionally, an increase in leakage diameter results in a sharp rise in hydrogen leakage per unit time. Notably, hydrogen demonstrates greater ease of diffusion in sandy soil compared to clay soil, leading to higher diffusion rates, concentrations, and ranges [23]. Li et al. [49] researched the influence of a temperature-stratified environment on the evolution characteristics and diffusion of hydrogen leakages. They found that in a temperature-stratified environment, leaked hydrogen tends to be trapped at a specific altitude and spreads horizontally, a phenomenon referred to as the "locking phenomenon." This research delved into the circumstances that will lead to this phenomenon by comparing hydrogen diffusion across various temperature gradients and leakage rates [49].

3 Methodology

This study used a comprehensive approach involving a literature review, interviews with experts, and a CFD model to address the research questions. The consulted experts included individuals from Gasunie for information on hydrogen transport characteristics, RIVM for potential environmental risks of hydrogen leakages, KWR for hydrogen-soil interactions, and Utrecht University for hydrogen leak detection and location methods.

The research framework illustrated in Figure 3.1, outlines the research steps undertaken in a top-to-bottom structure. This framework provides an overview of the methods used, categorized by the different categories: data collection, CFD modelling, and analyzing and concluding.

The goal of the CFD modelling was to find the hydrogen leakage rate based on the following parameters: leak size, pipe depth, groundwater level, and soil type. This leakage rate was used as input for the Monte Carlo analysis, which gave a probabilistic view of the financial and environmental effects of hydrogen leakages in high-pressure pipelines.

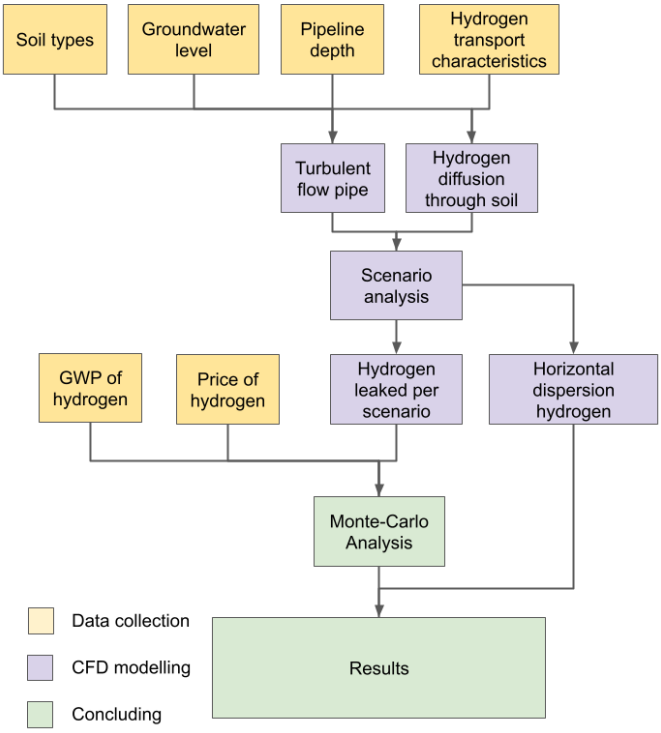

Figure 3.1: Research framework which contains the workflow of this research. The research framework has a top-to-bottom structure.

3.1 Hydrogen Backbone Environment

The data on groundwater levels and subsurface soil types obtained from DINOloket [25] was downloaded on 10-05-2024 and analyzed using QGIS, an open-source GIS software. In QGIS, the hydrogen backbone is superimposed on these maps to extract values of groundwater level and soil type around the backbone. This analysis helped identify the predominant soil types and groundwater levels in the area.

Subsequently, sand and clay were identified as the two most dominant soil types and therefore used in the CFD simulations. Additionally, the average values of the LG, Mean groundwater depth (MG), and Highest Groundwater depth (HG) were found and used as inputs for the groundwater level in the CFD simulations. Here the lowest depth is defined as the groundwater that is furthest away from the surface and the highest depth is the groundwater that is the closest to the surface.

A literature review and expert interviews provided additional relevant parameters such as permeability and porosity of the unsaturated and saturated soil types, which were essential for the CFD modeling.

3.2 Detection and Location Methods

A literature review was conducted to identify effective detection and location methods for hydrogen leakages in high-pressure pipelines. The review focused on examining existing technologies and methods used for gas leak detection. Each method is discussed on the following characteristics: working principles, leakage rate it can detect, upsides, downsides, and costs.

Gaining knowledge about these detection and location methods is important because then the leakage detection times can be estimated more accurately. The leakage detection times directly influence the total volume of hydrogen lost during a leak. Accurate and timely detection not only helps minimize the environmental impact and financial losses associated with hydrogen leakages but also enhances safety by reducing the potential for dangerous scenarios, such as explosions or fires. By identifying and evaluating the effectiveness of different detection techniques, this subsection aims to provide an understanding of the response times needed to address hydrogen leaks.

3.3 Simulation of Hydrogen Leak in Pipeline and Diffusion through Soil

The simulation of hydrogen leakage was conducted using Finite Element Method (FEM) software Comsol Multiphysics. FEM is a procedure for solving problems in physics by dividing a system into small simple parts, finite elements, which are consequently solved in relation to each other [50]. The simulation was divided into two parts: the pipeline leak and the subsequent diffusion through the soil. The schematic setup of the CFD model can be seen in Figure 3.2, where the asterisk marks the leak. Data on pipeline characteristics and hydrogen properties were sourced from literature and expert consultations, focusing

on parameters such as pressure, flow speed, and expected leak diameter. The following input parameters were used:

- Input pressure: 40 bar [16]
- Outlet velocity: 50 m/s [16]
- Pipe Diameter: 1 meter [16]
- Hydrogen Properties were taken from Comsol

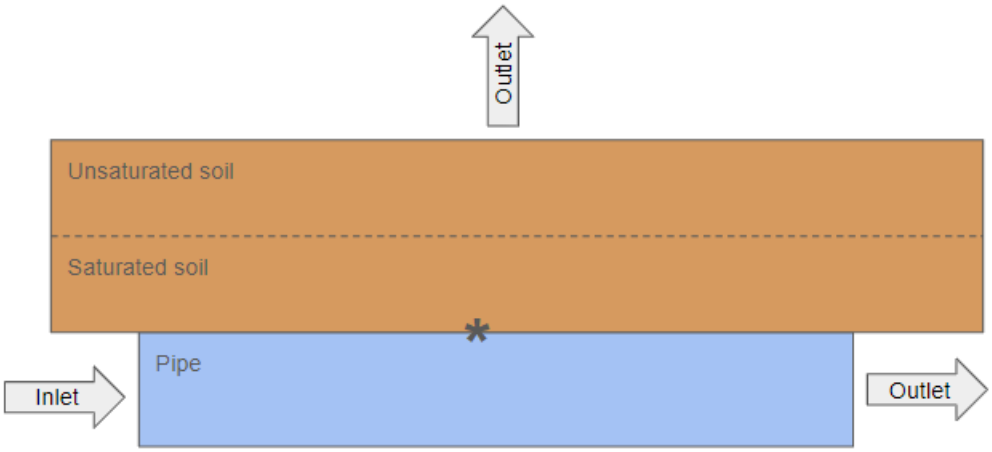

Figure 3.2: A schematic overview of the setup of the CFD model

3.3.1 Hydrogen flow pipe

The turbulent hydrogen flow through a 2D pipe was simulated using the $\kappa - \omega$ Low Reynolds number model in COMSOL Multiphysics [51]. This model is chosen since it can handle the high Reynolds numbers in the main part of the flow but it is also suitable for handling low Reynolds number flows near the wall where the velocity becomes zero. It can therefore accurately simulate the flow in the center as well as the flow near the walls of the pipe.

The κ-ω Low Reynolds number model was based on the following governing equations:

Continuity Equation
The continuity equation ensures the conservation of mass in the fluid flow. It dictates that the mass of fluid entering a control volume is equal to the mass leaving it [52; 53].

$$\nabla \cdot (\rho \mathbf{u}) = 0 \tag{3.1}$$

where ρ is the fluid density, and $\mathbf{u}$ is the velocity vector.

Momentum Equation
The momentum equation describes how momentum is conserved in fluid flow. This equation considers the different forces acting on the fluid, such as pressure, friction (viscous stresses), and external forces like gravity [52; 53].

$$\rho(\mathbf{u} \cdot \nabla)\mathbf{u} = \nabla \cdot [-p\mathbf{I} + \mathbf{K}] + \mathbf{F} \tag{3.2}$$

where p is the pressure, $\mathbf{I}$ is the identity matrix, $\mathbf{K}$ is the stress tensor, and $\mathbf{F}$ is the body force vector.

$$\mathbf{K} = (\mu + \mu_T)\left(\nabla\mathbf{u} + (\nabla\mathbf{u})^T\right) - \frac{2}{3}(\mu + \mu_T)(\nabla \cdot \mathbf{u})\mathbf{I} - \frac{2}{3}\rho k\mathbf{I} \tag{3.3}$$

where μ is the dynamic viscosity, μ_T is the turbulent (eddy) viscosity, and k is the turbulent kinetic energy.

Turbulent Kinetic Energy Equation
The turbulent kinetic energy equation describes the evolution of the kinetic energy associated with the turbulent fluctuations in the fluid flow. It tracks the generation, dissipation, and transport of turbulent energy, which helps model the energy exchange between the large-scale flow and the small-scale turbulent eddies. This equation is particularly important in capturing the effects of turbulence on hydrogen dispersion and mixing within the pipe [53; 54].

$$\rho(\mathbf{u} \cdot \nabla)k = \nabla \cdot [(\mu + \mu_T\sigma_k^*)\nabla k] + P_k - \beta_0^*\rho\omega k \tag{3.4}$$

where σ_k^* is a model constant, P_k is the production term of turbulent kinetic energy, β_0^* is another model constant, and ω is the specific dissipation rate. The equations or values for the model constants can be found in Appendix A.

Specific Dissipation Rate Equation
The specific dissipation rate equation governs the rate at which turbulent kinetic energy is converted into thermal energy, primarily through the dissipation of small-scale turbulent structures. This equation plays an important role in closing the turbulence model and accurately representing the energy balance within the system.[53; 54].

$$\rho(\mathbf{u} \cdot \nabla)\omega = \nabla \cdot [(\mu + \mu_T\sigma_\omega)\nabla\omega] + \alpha\frac{\omega}{k}P_k - \beta_0\rho\omega^2 \tag{3.5}$$

where σ_ω and β_0 are model constants, and α is a coefficient.

Turbulent Viscosity
The turbulent viscosity equation defines the eddy viscosity, which represents the enhanced momentum transport due to turbulence. In the context of this research, this equation helps quantify the additional mixing and momentum transfer caused by turbulence, which affects the overall flow dynamics [53; 54].

$$\mu_T = \frac{\rho k}{\omega} \tag{3.6}$$

Production Term of Turbulent Kinetic Energy
The production term of turbulent kinetic energy quantifies the rate at which kinetic energy from the mean flow is transferred to the turbulent eddies. This term is necessary for sustaining turbulence in the flow, as it describes the continuous energy transfer that drives the chaotic motion of the fluid [53; 54].

$$P_k = \mu_T \left[\nabla \mathbf{u} : (\nabla \mathbf{u} + (\nabla \mathbf{u})^T)\right] - \frac{2}{3}(\nabla \cdot \mathbf{u})^2 \rho k \tag{3.7}$$

These equations collectively enabled the simulation of turbulent hydrogen flow through a pipe, capturing the essential dynamics from the bulk flow to the near-wall regions where low Reynolds numbers were significant [53; 52; 54].

the model had the following inputs

Wall

The walls had a no-slip boundary condition, which effectively meant that the velocity was zero at the wall. The equations used were:

$$\mathbf{u} = 0 \tag{3.8}$$

This meant that the velocity was zero at the boundary.

$$k = 0, \quad \omega = \lim_{\ell_w \to 0} \frac{6\nu}{\beta_0 \ell_w^2}, \quad \ell_w = 0 \tag{3.9}$$

This indicated that the turbulent kinetic energy was zero, and the specific dissipation rate ω approached a limiting value as the wall distance ℓ_w went to zero. Here, ν was the kinematic viscosity and β_0 was a model constant.

Inlet

The inlet was defined as a fully developed flow at 40 bar. The fully developed flow boundary condition was visualized in Figure 3.3.

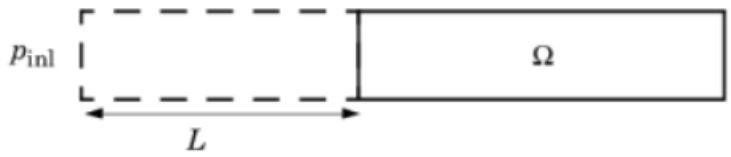

Figure 3.3: Visualisation of the fully developed flow boundary condition in Comsol

The flow entered the domain Ω through a straight channel of length L. This channel was an extension of the inlet cross-section, where the constant pressure P_{inl} of 40 bar was applied. The boundary condition specified that the tangential flow component at the boundary was zero.

The length L was chosen to be ten times the inlet edge length. This setup allowed the actual velocity profile at the inlet to adapt to the solution inside the computational domain.

The following equations were used:

$$\mathbf{u} \cdot \mathbf{t} = 0 \tag{3.10}$$

Where $\mathbf{t}$ is the tangential vector. This means that the velocity at the boundary was perpendicular to the boundary (so there was no velocity moving along the boundary)

$$[-p\mathbf{I} + \mathbf{K}]\mathbf{n} = -p_{\text{grad}}\mathbf{n} \tag{3.11}$$

where p_{grad} is the pressure gradient.

This represented the balance of forces at the boundary where the pressure gradient balanced the normal component of the stress.

Outlet

The outlet was defined as a fully developed flow with an average velocity of 50 m/s. This was slightly lower than the maximum allowed flow velocity of 60 m/s and depended on demand [16]. The principle of the fully developed flow as an outlet boundary condition was the same as for the inlet boundary condition.

The following equations were used:

$$\nabla k \cdot \mathbf{n} = 0, \quad \nabla \omega \cdot \mathbf{n} = 0 \tag{3.12}$$

This indicated that there was no flux of turbulent kinetic energy and specific dissipation rate across the boundary.

$$\mathbf{u} \cdot \mathbf{t} = 0 \tag{3.13}$$

This meant that the tangential component of the velocity was zero at the boundary.

$$[-p\mathbf{I} + \mathbf{K}]\mathbf{n} = -p_{\text{grad}}\mathbf{n} \tag{3.14}$$

This represented the balance of forces at the boundary where the pressure gradient balanced the normal component of the stress.

Leak

A linear extrusion coupling operator was used to couple the velocity and pressure of the leak in the pipe to the inlet source for the soil. A Linear Extrusion coupling operator mapped an expression from a source to a destination. This operator was used to define a linear mapping. The mapping process started by projecting the destination orthogonal onto the linear space spanned by its vertices. This space was then mapped linearly to the source, aligning each destination vertex with its corresponding source vertex.

With this linear extrusion coupling operator, the velocity field of the leak point in the pipe was coupled to the soil's inlet velocity, and the soil's pressure at the leak point was coupled to the pressure outlet of the leak point in the pipe. A schematic overview of the linear extrusion coupling can be found in Figure 3.4.

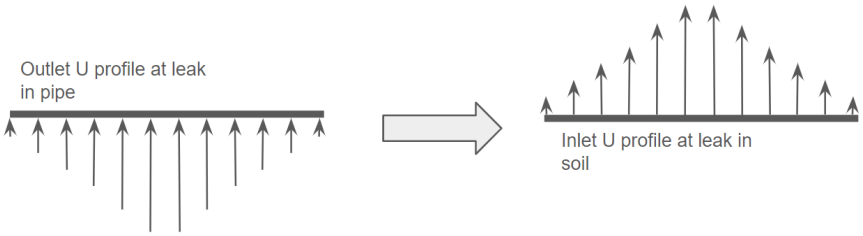

Figure 3.4: A schematic overview of the linear extrusion coupling between the leak point in the pipe defined as an outlet in the turbulent flow physics and the defined inlet boundary in the porous media physics

The following equations were used:

$$[-p\mathbf{I} + \mathbf{K}]\mathbf{n} = -\hat{p}_0\mathbf{n} \tag{3.15}$$

This represented the balance of forces at the boundary where the normal component of the stress was balanced by the reference pressure $\hat{p}_0$ which was set to be equal to the downward pressure of the soil.

$$\hat{p}_0 \leq p_0 \tag{3.16}$$

This indicated that the pressure at the boundary (p_0) was always less or equal to the set boundary pressure ($\hat{p}_0$).

$$\nabla k \cdot \mathbf{n} = 0, \quad \nabla\omega \cdot \mathbf{n} = 0 \tag{3.17}$$

This indicated no flux of turbulent kinetic energy and specific dissipation rate across the boundary.

3.3.2 Hydrogen flow soil

The Brinkman equations and the Forchheimer flow model were employed to simulate hydrogen flow through the soil, which was treated as a homogeneous porous medium. The Brinkman equations build upon Darcy's law by incorporating the effects of viscous shear, which refers to the frictional forces that occur within the fluid as it moves through the tiny spaces in the porous material. These forces cause the fluid layers to resist sliding past one another, leading to energy dissipation. This extension makes the Brinkman equations particularly well-suited for modeling scenarios where the flow is relatively fast, as it accurately captures the additional resistance encountered in such conditions [55; 56].

In addition to viscous shear, the Forchheimer term was included to account for inertial effects, which become significant at higher flow velocities. Inertial effects refer to the tendency of the fluid to resist changes in its motion due to its mass. The Forchheimer term addresses these effects, ensuring that the model remains accurate even at higher velocities [57; 58]. The modified equation is:

$$\mathbf{u} = -\frac{\kappa}{\mu}\nabla p - \beta\rho|\mathbf{u}|\mathbf{u} \tag{3.18}$$

where: β is the Forchheimer constant, and $|\mathbf{u}|$ is the magnitude of the Darcy velocity.

The Forchheimer term $\beta\rho|\mathbf{u}|\mathbf{u}$ accounted for the inertial losses that were not captured by the linear Darcy's term.

The governing equations in the Brinkman equations were:

Continuity Equation

$$\nabla \cdot (\rho\mathbf{u}) = Q_m \tag{3.19}$$

Momentum Equation

$$0 = \nabla \cdot (-p\mathbf{I} + \mathbf{K}) - \left(\mu\kappa^{-1} + \beta\rho|\mathbf{u}| + \frac{Q_m}{\epsilon_p^2}\right)\mathbf{u} + \mathbf{F} \tag{3.20}$$

Where κ was the permeability of the porous medium, β was the Forchheimer constant, Q_m a source term, ϵ_p the porosity, and $\mathbf{F}$ was the volume force.

The volume force $\mathbf{F}$ was included to mimic gravity and was calculated with the following equation:

$$\mathbf{F} = -g * \rho \tag{3.21}$$

where g was the gravity constant of 9.81 m/s^2, and ρ was the density which was equal to 2000 kg/m^3 for unsaturated sand [59] and 2200 kg/m^3 for unsaturated clay [60].

$$\mathbf{K} = \mu \frac{1}{\epsilon_p} \left(\nabla \mathbf{u} + (\nabla \mathbf{u})^T \right) - \frac{2}{3} \mu \frac{1}{\epsilon_p} (\nabla \cdot \mathbf{u}) \mathbf{I} \tag{3.22}$$

$$\beta = \frac{c_F}{\sqrt{\kappa}} \tag{3.23}$$

Where c_F was the dimensionless Forchheimer coefficient, which was set to 0.55 for sand [61] and to 0.15 for clay [62]. The Forchheimer constant accounted for the inertial effects in the porous medium.

The permeability of the dry medium was calculated with the Ergun equation:

$$\kappa_{dry} = \frac{d_p^2}{150} \cdot \frac{\epsilon_p^3}{(1 - \epsilon_p)^2} \tag{3.24}$$

where d_p was the particle diameter. Both values for the particle diameter and porosity were found in the literature or approximated from the literature.

The permeability of the wet soil was calculated using the relative permeability value κ_{rg}:

$$\kappa_{wet} = \kappa_{dry} * \kappa rg \tag{3.25}$$

The values for the relative permeability were found in the literature and were equal to 0.05 [63; 64] and 0.01 [65] for sand and clay, respectively.

Wall

The same condition as mentioned in subsection 3.3.1 was used here. As a result of the lack of turbulence, the only equation implemented was equation 3.8.

The block of soil was made wide enough that the walls did not impact the dispersion of hydrogen through the soil.

Inlet

The inlet was coupled to the leak point in the pipe through linear extrusion coupling.

$$\mathbf{u}_3 = \mathbf{u}_0 \tag{3.26}$$

where $\mathbf{u}_3$ was the velocity at the inlet, and $\mathbf{u}_0$ was the specified inlet velocity which was equal to the velocity in the leak point of the pipe in the turbulent flow physics.

Outlet

The top of the soil was defined as an outlet with an atmospheric pressure of 1 atm. The following equations governed the outflow of hydrogen:

$$-p\mathbf{I} + \mathbf{K}]\mathbf{n} = -\hat{\rho}\hat{\mathbf{n}} \tag{3.27}$$

$$\hat{p}_a \leq p_0 \tag{3.28}$$

This indicated that the pressure at the boundary (p_0) was always less or equal to the set boundary pressure ($\hat{p}_a$, which was equal to the atmospheric pressure).

3.4 Scenarios Simulation

Different scenarios are simulated in Comsol to find the impact of the size of leaks, groundwater level, pipe depth, and soil type. An overview of the different parameters used can be seen in Table 1

Table 1: An overview of the different values used for every variable

Size of leaks (cm)	**Groundwater level** (m)	**Depth of pipe (m)**	**Soil type**
0.25	0.65 (HG)	1.25	Sand
0.5	1.1 (MG)	1.75	Clay
1	1.54 (LG)	2.25	
2			
3			

where the HG, MG, and LG were found in subsection 3.1. The depths were based on the average pipe depth of 1.75 m and the minimum allowed pipe depth of 1 m as discussed in subsection 2.2. This totaled 90 simulations run in Comsol. The main output of these simulations was the percentage of hydrogen leaked and the velocity profile at the boundary between the soil and the atmosphere.

3.5 Impacts of Hydrogen Leakages

The impact of the hydrogen leakages was evaluated on three points:

1. Environmental impact
2. Financial impact
3. Safety risk

The GWP of hydrogen, discussed in subsection 2, was used as a measure for the environmental impact of hydrogen leaks. The GWP of the same amount of energy generated by burning natural gas was also calculated for comparison.

The financial impact was assessed by estimating the price of hydrogen per kg for different years based on literature, multiplied by the amount of hydrogen leaked in kg.

For the flammability risk, the horizontal dispersion of hydrogen in each scenario was identified. This helped assess the range from which hydrogen was leaking into the atmosphere and if there was any danger of hydrogen-fueled fire. This was calculated by determining the horizontal distance from the centre of the leak to the point where the velocity was equal to 0.5 m/s. According to Malakhov et al. [66]; Hartmann et al. [67]; Depken et al. [68], a leak velocity between 0.1 and 1 m/s ensured the hydrogen concentration stayed below the flammable limits. In this research, a limit of 0.5 m/s was chosen.

3.6 Monte-Carlo Analysis

Due to uncertainties in the amount and size of leaks, soil type, groundwater level, and pipe depth, Monte Carlo analysis was used to provide a statistical distribution of possible outcomes. This method involves running numerous simulations with random inputs sampled from probability distributions representing the uncertainty in system parameters. A schematic overview of the steps in the Monte Carlo analysis can be seen in Figure 3.5. It shows the data sources consulted for each component and the relations between those. Each step will be discussed and explained below.

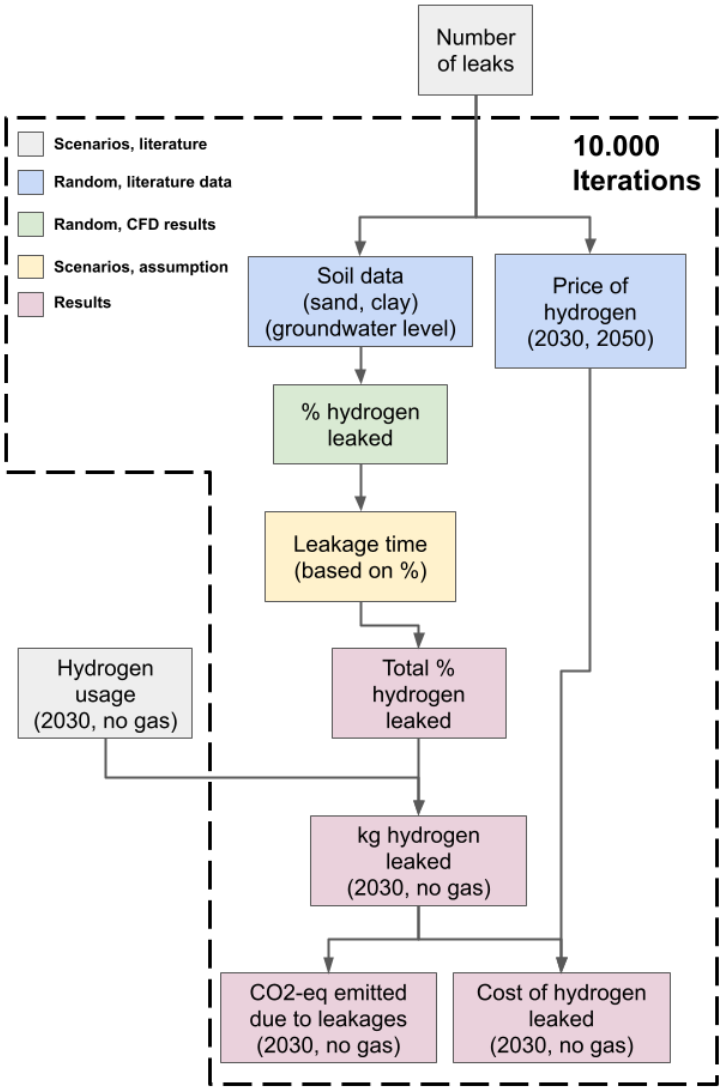

Figure 3.5: Schematic overview of the different steps of the Monte Carlo analysis

An expected number of leaks per year of 1 is used. This choice is based on historical data from European Gas Pipeline Incident Data Group (EGIG) [69] on leak frequencies in high-pressure natural gas transport pipelines across Europe. It was chosen to use historical data as this reflects the higher occurrences of leakages due to the technology being less developed. The average from 1970-1975 is chosen because the maturity of the natural gas transport technique at that time can be compared to the current maturity of hydrogen transport through pipelines (especially pure hydrogen). European Gas Pipeline Incident Data Group (EGIG) [69] considers seventeen gas transmission system operators, including Gasunie, and found that in the earliest years (1970 to 1975), the average leakage rate was 0.86 leakages per year per thousand km. Given that approximately 1200

km of hydrogen pipeline is expected [16], this would equal approximately 1 leakage per year.

The soil data considered in the Monte Carlo analysis focused on the two most common soil types near the hydrogen backbone: sand and clay. The ratios found for these soil types were normalized, and the probabilities for each soil type were incorporated into the analysis. Regarding groundwater levels, three measuring points were used: LG, MG, and GHG. The probability of a leak occurring in each groundwater level was set to 0.25, 0.5, and 0.25, respectively, because LG and GHG represent extreme seasonal values (summer and winter), whereas MG represents the average condition during the year, occurring more frequently (spring and autumn).

The price of hydrogen was estimated based on five scenarios considering green, grey, and blue hydrogen over two different time scales, 2030 and 2050. The expected mix of hydrogen types and their respective estimated prices for 2030 and 2050 were used. Specifically, the mix for 2030 is expected to be 55% grey, 35% blue, and 10% green hydrogen, while for 2050, the mix is projected to be 0% grey, 25% blue, and 75% green hydrogen [70; 71]. Table 2 provides an overview of the expected hydrogen prices per kg for both years, grouped by type of hydrogen.

Table 2: An overview of the expected hydrogen prices per kg for 2030 and 2050 grouped per type of hydrogen [72]

		Grey	**Blue**	**Green**
2030	**Low**	€0.50	€1.00	€1.80
	Low Average	€1.00	€1.75	€1.68
	Average	€2.13	€2.63	€3.18
	High Average	€3.25	€3.50	€4.67
	High	€4.00	€6.00	€5.00
2050	**Low**	€0.50	€1.00	€1.00
	Low Average	€0.88	€1.67	€1.42
	Average	€2.56	€2.46	€2.43
	High Average	€4.25	€3.25	€3.43
	High	€5.50	€5.50	€3.80

A random scenario was selected from the 90 CFD simulations, corresponding with the chosen soil type and groundwater level. This scenario provided the percentage of hydrogen leaked, which was then used to calculate the total percentage of hydrogen leaked in a year.

Given the absence of specific data on leakage detection and location, several assumptions were made to estimate leakage time:

- If the leakage rate is 10% or higher, the leak is assumed to be detected immediately. However, due to the time required to shut down the transmission network the leakage time is chosen randomly between 2 and 12 hours for each iteration.
- If the leakage rate is between 5% and 10%, there is a 20% chance of immediate

detection. If detected, the random time between 2 and 12 hours is used. If not, detection must occur through intermittent inspection (e.g., aerial or ground surveillance), with the leakage time chosen randomly between 1 and 14 days for each iteration. This interval is chosen because Gasunie performs inspections biweekly [22]

- If the leakage rate is less than 5%, there is a 10% probability of immediate detection. If detected, the same random time between 2 and 12 hours is applied. If not, detection through intermittent inspection is necessary, and the leakage time is randomly set between 1 and 14 days for each iteration.

To transform the percentage leaked found from the Monte Carlo analysis to kg of hydrogen leaked, two scenarios were considered to estimate the absolute amount of hydrogen leakage. The first scenario was based on the projected hydrogen usage in 2030, estimated at 100 PJ per year [13]. The second scenario assumed a complete substitution of natural gas with hydrogen in the Netherlands, which equated to 997.096 PJ per year [73]. These scenarios were used to calculate the absolute amounts of hydrogen leaked.

For each iteration of the Monte Carlo analysis, the amount of hydrogen lost in kg was multiplied by the GWP100 of hydrogen (16.5 Ocko and Hamburg [44]). The financial impact of hydrogen leakage was calculated by multiplying the cost per kg of hydrogen by the amount of hydrogen lost. The cost of hydrogen differs per iteration of the Monte Carlo analysis since there were different price scenarios considered.

3.7 Sensitivity Analysis

While the Monte Carlo analysis provided a framework to account for uncertainties in factors such as leak size, groundwater level, and pipe depth, it relies on predefined probability distributions to model these uncertainties. The accuracy and reliability of the Monte Carlo analysis outcomes are determined by the sensitivity of these distributions. Therefore, a sensitivity analysis was conducted to evaluate how variations in the input distributions could affect the results of the Monte Carlo analysis. The goal of this sensitivity analysis was to identify the impact of different distribution assumptions on the overall model output and to determine which parameters exerted the most significant influence on the results.

In this sensitivity analysis, the following parameters were varied: the number of leaks, the immediate detection time, the non-immediate detection time, the ratio of the leaked percentage that is detected immediately, and the leak rate from which a leak is detected immediately. The immediate detection time refers to scenarios where leaks are identified through continuous monitoring methods, while the non-immediate detection time refers to scenarios where leaks are identified through intermittent detection methods. This distinction highlights the varying effectiveness of different detection approaches in locating leak events. These variations provided insights into the relative importance of each parameter and their contribution to the overall uncertainty of the model. These parameters were chosen because of the lack of data and information regarding these

parameters.

The base case setup, as detailed in subsection 3.6, served as a reference point for comparison. For the sensitivity analysis, a range of values for the number of leaks was considered: 0.25, 0.5, 1, 2, 5, and 10. More variation was included in the upward trend than in the downward trend to account for two considerations: (a) the less mature status of hydrogen transport through high-pressure pipelines, and (b) the higher tendency for hydrogen to leak compared to natural gas [74; 21]. For the remaining parameters, values representing 25%, 50%, 75%, 100%, 125%, 150%, and 175% of the base case were examined.

The result of this sensitivity analysis was analyzed based on four characteristics: the mean percentage of hydrogen leaked, the 95^{th} percentile (P_{95}) of hydrogen leaked, the mean cost incurred due to leakages, and the mean CO_2-eq emitted due to leakages. For the last two characteristics, the 2030 scenario was included to indicate the financial and environmental impact.

4 Results and Discussion

4.1 Hydrogen Backbone Environment

Figure 4.1 shows the relative occurrence of each soil type near the hydrogen backbone. Sand and clay are the most occurring soil types, respectively 27 and 21 %. These values were then normalized to assume that all the soil is either sand or clay, and this probability was used to find either sand or clay in the Monte Carlo analysis. This probability is found to be 57% for sand and 43% for clay.

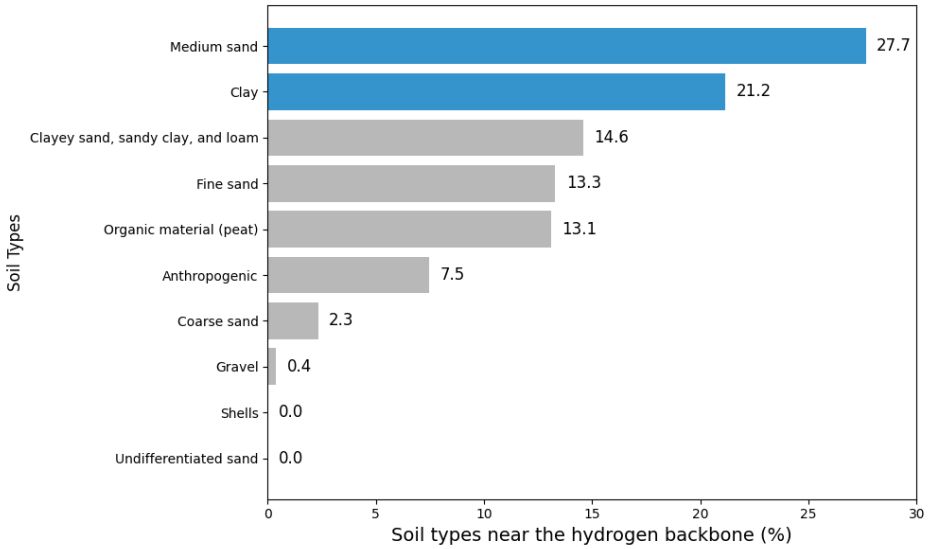

Figure 4.1: The relative occurrence of each soil type near the hydrogen backbone, normalized for the points with missing data [25]

Figure 4.2 shows the mean value of the measured groundwater levels (LG, MG, and HG) near the hydrogen backbone. The values of LG, MG, and HG are respectively equal to 1.54 m, 1.1 m, and 0.61 m. This is the distance measured from the surface level down to the groundwater. This is why the HG is the smallest number.

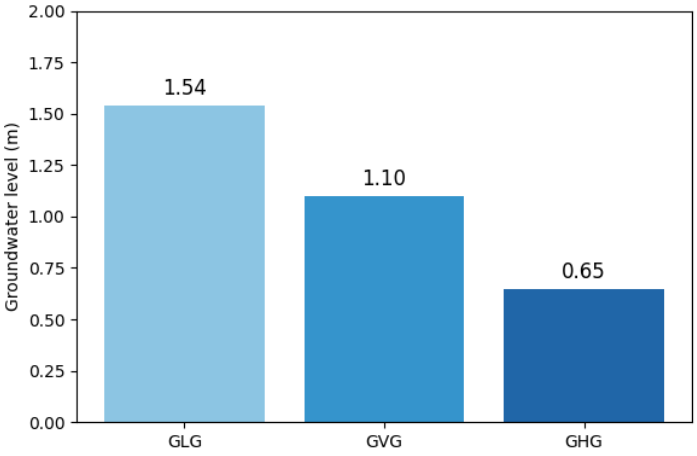

Figure 4.2: The mean LG, MG, and HG near the hydrogen backbone [25]

4.2 Detection and Location Methods

The effectiveness of various hydrogen pipeline leak detection methods was analyzed based on their working principles, accuracy, ability to pinpoint leaks, costs, and drawbacks. The methods can be categorized into the following classifications [75]:

1. Externally based methods: these methods rely on external sensors or devices to physically detect leaks outside of the pipeline.
2. Visual/Inspection methods: these methods involve manual inspection of pipelines at regular intervals.
3. Internally/Computational based methods: these methods use internal data such as pressure, flow rate and temperature from within the pipe and analyze this through computational models and algorithms.

The categorization of the different techniques can be seen in Figure 4.3.

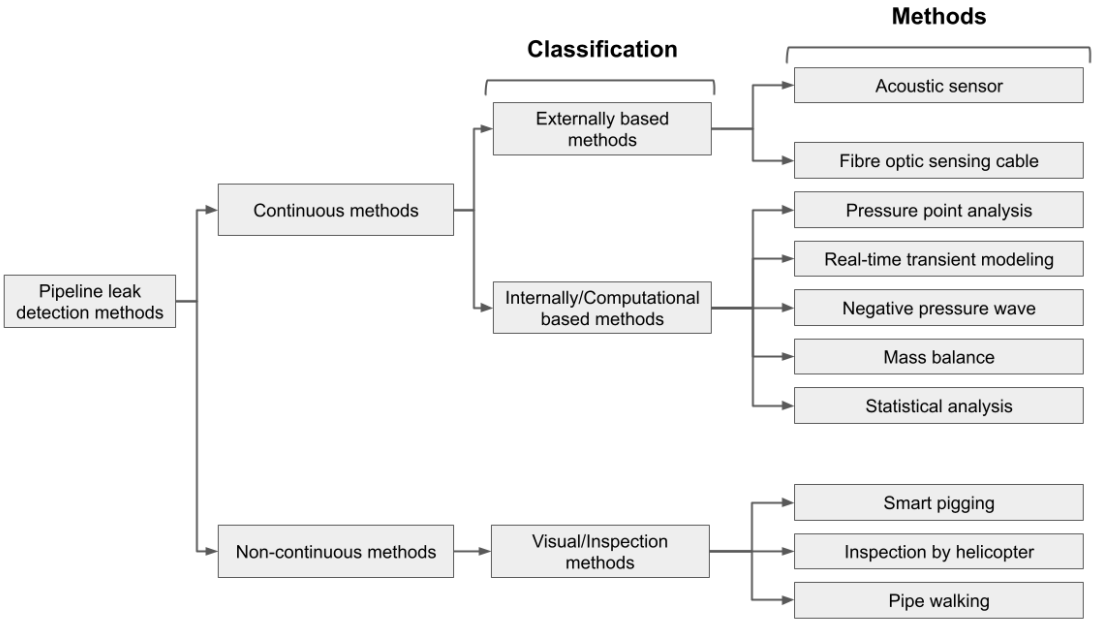

Figure 4.3: Categorization of detection methods for leaks in pipelines

In Tables 3, 4, and 5 a brief overview of different detection methods is given. Each method is described on the working principles, the detected leakage rate (if known), upside, downside, and relative costs.

Table 3: An overview of the externally based detection methods

Method	**Working Principle**	**Detected Leakage Rate**	**Upside**	**Downside**	**Cost**	**Citations**
Acoustic Methods	Detects acoustic waves from gas escaping a pipeline	0.9% leakage rate in lab settings	High sensitivity, real-time monitoring, effective in remote areas	False alarms due to noise, high sensor cost for long pipelines	Expensive (sensor costs)	[76; 77; 78; 79; 80]
Optical Fiber Sensing (OFS)	Uses fiber optic cables to detect acoustic/temperature changes	0.4 m^3/min over 50 km	Continuous monitoring, high spatial resolution, immune to EMI	Sensitive to noise, high setup/-maintenance cost, fragile fibers	Expensive (setup/-maintenance)	[81; 82; 83]

Table 4: An overview of internally based detection methods

Method	Working Principle	Detected Leakage Rate	Upside	Downside	Cost	Citations
PPA	Monitors pressure drops at various pipeline points	-	Rapid response, simple setup, suitable for various configurations	High false positives, many sensors needed, limited localization	Moderate (sensor costs)	[84; 85; 86]
RTTM	Compares real-time sensor data with a detailed pipeline model	<1% of flow	Precise detection/localization, predictive capability	Complex, high cost, inaccurate with poor model	Expensive (modeling/computational costs)	[87; 88; 89]
NPW	Detects pressure waves caused by sudden drops from leaks	0.48% of total flow rate (in combination with Mass Balance)	Quick, accurate detection, low setup cost, real-time capability	Susceptible to noise, less effective for small leaks, complex calibration	Moderate (sensor costs)	[90; 91; 92; 93]
Mass Balance Method	Calculates difference between input and output mass/volume	1.1% minimum leakage rate	Simple, low-cost, quick detection	Poor localization, sensitive to noise, ineffective for small leaks	Low (minimal instruments)	[94; 95; 96]
Statistical Methods	Analyzes sensor data deviations from normal operation	0.5-10% of inlet flow rate	Adaptable, handles multiple leaks, automated	High computational needs, requires extensive training data	Moderate (computational resources)	[97; 98; 99; 100]

Table 5: An overview of the visual/Inspection detection methods

Method	Working Principle	Detected Leakage Rate	Upside	Downside	Cost	Citations
Smart Pigging	Uses smart devices inside pipelines to assess conditions	Preventive measure	Detailed internal assessment, continuous monitoring, safety	Expensive equipment, complex data analysis, limited by pipeline design	Expensive (equipment/personnel)	[101; 102]
Inspection by Helicopter	Helicopters with sensors measure air refractive index changes	2 l/min (highly dependent on environmental factors)	High accuracy, no operation stoppage required	High operational cost, weather dependent	Expensive (operational costs)	[103; 104; 105]
Pipe Walking	Personnel manually inspect pipelines with gas sniffers	from 15 ppm (depending on sensor used)	Simple, low equipment costs	Time-consuming, expensive manpower, limited reach	Moderate (manpower costs)	[106; 104; 107]

In conclusion, each hydrogen leak detection method presents unique strengths and limitations. The choice of method often depends on the specific requirements of the pipeline network, including the need for real-time monitoring, cost constraints, environmental considerations, and the desired accuracy in detecting and locating leaks. Combining multiple methods often provides the best overall protection by leveraging the complementary strengths of each technique. Gasunie was unwilling to provide details about which methods they are intending to implement. Therefore, in the rest of this study assumptions had to be made on detection times.

4.3 Grid Independence

To evaluate the grid independence, the computational domain was divided into five grid levels: 201,600, 276,598, 410,770, 908,416, and 1,177,986 to monitor the hydrogen velocity through a hole with a diameter of 0.5 cm, as shown in Figure 4.4. When the number of grids reached 410,770, the average relative error of hydrogen velocity through the

hole was within 1.5%. The 410,770 grid level was selected for numerical simulation to ensure calculation accuracy and minimise computational time. This approach aligns with best practices in computational fluid dynamics, as suggested by several studies [108; 109].

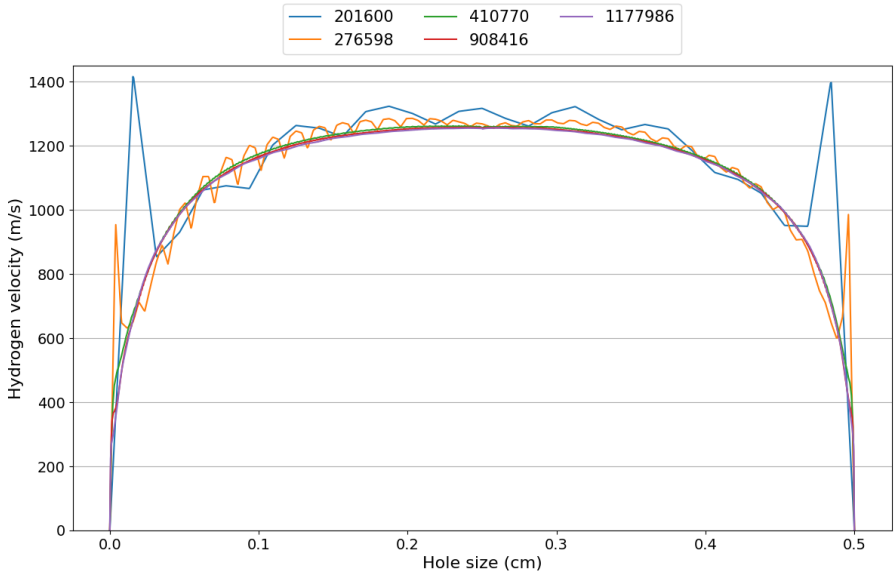

Figure 4.4: Grid independence verification

4.4 Impact Different Scenarios

Figure 4.6 illustrates the percentage of hydrogen leakage in various scenarios where the pipeline is surrounded by sand. The scenarios are characterized by three different pipe depths (1.25 m, 1.75 m, and 2.25 m) and three groundwater levels (LG, MG, and HG). The results indicate that the most significant factor influencing hydrogen leakage is the presence of either saturated or unsaturated soil at the boundary of the pipe. When the pipe is above the groundwater level, hydrogen leaks more easily due to the higher permeability of the unsaturated soil. In contrast, when the pipe is below the groundwater level, hydrogen encounters saturated soil, which has lower permeability and restricts leakage [110].

However, the variation in leakage rates is relatively small across different pipe depths and groundwater levels when the pipe is submerged. This minimal difference can be attributed to the fact that the leakage rate is measured at the boundary of the hole, directly at the interface between the pipe and the surrounding soil. Thus, the immediate condition of the soil, whether saturated or unsaturated, has a more pronounced impact on leakage than the overall size of the saturated zone or the pipe's depth. The slight decrease in leakage observed with increasing pipe depth likely results from the slightly longer pathway that hydrogen travels through the porous media.

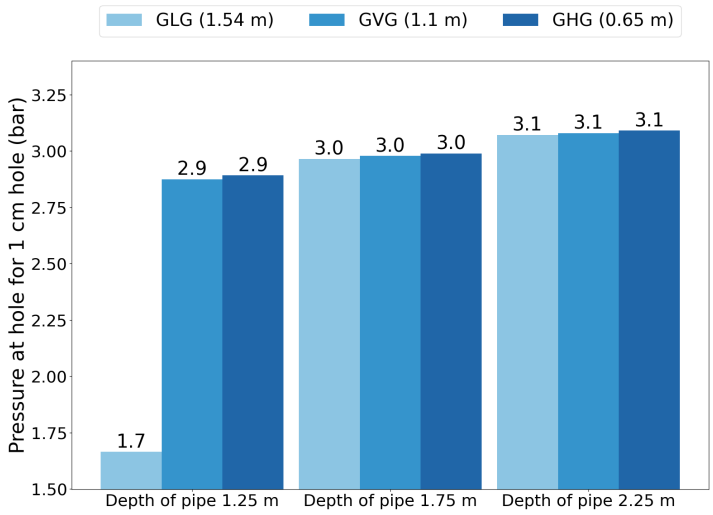

Figure 4.5: The pressure at the boundary between the pipe and the soil

Figure 4.5 shows the pressure build-up at the boundary between the hole and the surrounding soil, indicating the conditions right at the point of leakage. It shows that when the pipeline is submerged, the pressure build-up is approximately the same across different scenarios. Since the leakage process is primarily driven by pressure, this observation suggests that leakage rates should be similar for all submerged scenarios. This consistency in leakage rates is also reflected in Figure 4.6.

The similar pressure build-up across submerged scenarios can be explained by the permeability encountered by hydrogen as it escapes through the pipeline. When hydrogen leaks, a pressure build-up occurs because hydrogen tries to flow through a permeable zone. Since the permeability value for each submerged scenario remains constant at the boundary, the pressure build-up and resulting leakage rates are also consistent.

The decision to measure leakage rates at the boundary between the pipe and soil was made to effectively capture the actual leakage occurring from the pipeline, as this is a direct indicator of the loss of hydrogen, both in terms of environmental impact and financial costs. Furthermore, since the soil is simulated as a porous medium without a reaction term, every kilogram of hydrogen that leaks through this boundary will inevitably end up in the atmosphere. This approach ensures that all hydrogen escaping from the pipeline is accounted for, providing an accurate assessment of leakage for safety, economic, and environmental considerations.

Figures 4.6a to 4.6e show that the hole size is the most critical factor affecting hydrogen leakage. For instance, in the scenario with a hole size of 3 cm, up to 27% of the transported hydrogen can be lost, highlighting the importance of robust leak detection systems. Even minor leaks can lead to substantial hydrogen loss, emphasizing the necessity for effective leakage detection methods to ensure pipeline efficiency and safety [111; 112].

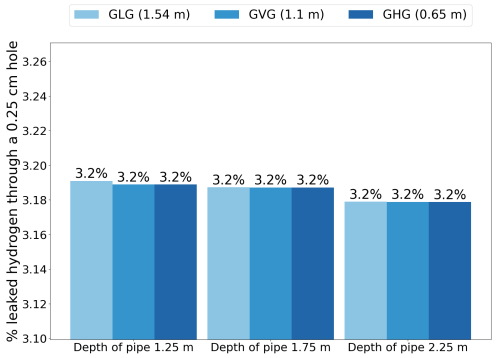

(a) Hole size 0.25 cm

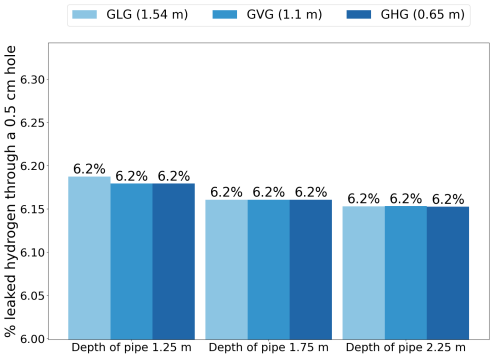

(b) Hole size 0.5 cm

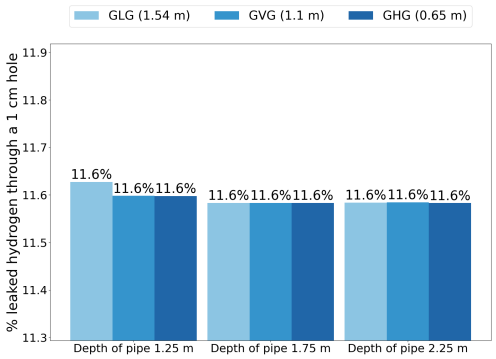

(c) Hole size 1 cm

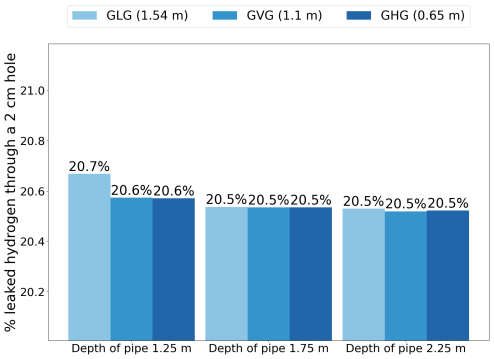

(d) Hole size 2 cm

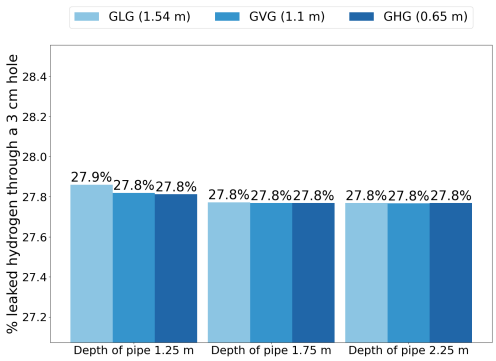

(e) Hole size 3 cm

Figure 4.6: The percentage of hydrogen leaked through sand for different depths of pipes and groundwater levels.

Figure 4.7 presents the percentage of hydrogen leakage for scenarios where the pipeline is surrounded by clay. While the impact of different scenarios on hydrogen leakage remains modest, it is slightly more noticeable than in sand. This difference is due to clay's

lower permeability than sand, as clay has larger pore sizes and higher water retention capabilities. These properties restrict hydrogen flow more in clay than in sand, making clay more sensitive to changes in pipe depth and groundwater levels [113]. Consequently, even minor changes in environmental conditions can lead to more significant variations in leakage rates in clay than in sand, where hydrogen flow is less restricted.

Additionally, similar to the observations with sand, there is a significant increase in hydrogen leakage in the scenario where the pipeline is not submerged and the hole size remains the most critical parameter influencing the amount of hydrogen leaked.

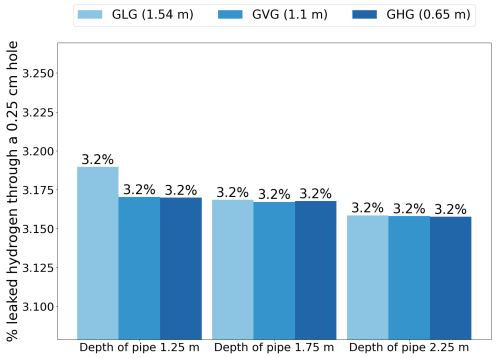

(a) Hole size 0.25 cm

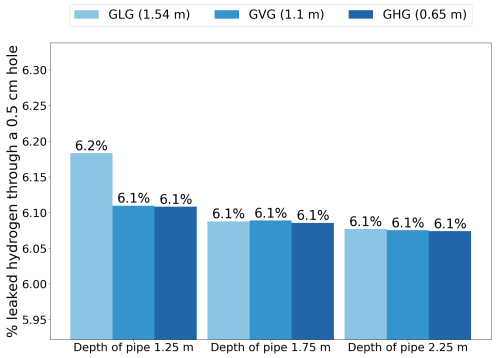

(b) Hole size 0.5 cm

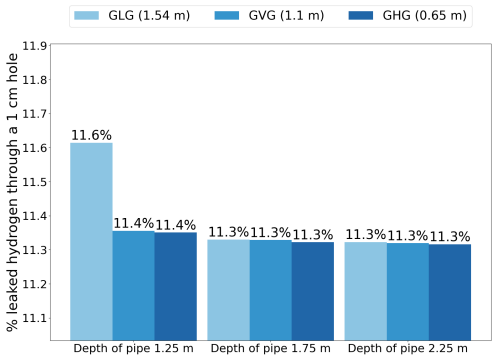

(c) Hole size 1 cm

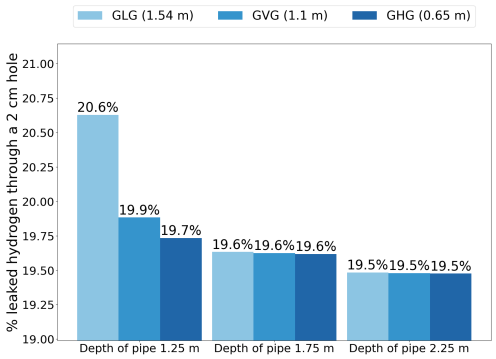

(d) Hole size 2 cm

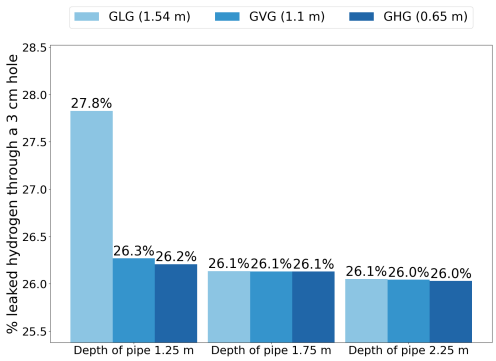

(e) Hole size 3 cm

Figure 4.7: The percentage of hydrogen leaked through clay for different depths of pipes and groundwater levels

Figures 4.8a and 4.8b provide insight into the impact of pipe depth and groundwater levels on the hydrogen velocity profiles at the boundary between soil and atmosphere. The first figure, 4.8a, shows the velocity profile for different pipe depths in a MG scenario

with a leak size of 1 cm. The results demonstrate that pipe depth significantly influences hydrogen dispersion into the atmosphere. Hydrogen travels a longer path through the soil with increased pipe depth, allowing more time for horizontal diffusion. This effect is reflected in the broader and lower peaks for deeper pipes, as opposed to the higher and narrower peaks observed with shallower pipes. Additionally, clay consistently shows lower velocity profiles than sand due to its lower permeability.

The second figure, 4.8b, illustrates the velocity profile for different groundwater levels, maintaining an average pipe depth and a leak size of 1 cm. Higher groundwater levels result in increased peak velocities but with narrower profiles. This pattern is attributed to the longer distance hydrogen must travel through saturated soil, which has a lower permeability. As a result, to take the path of least resistance, the hydrogen moves more directly upwards. Notably, the initial segment of the saturated zone has the most significant effect on the flow rate into the atmosphere, as the differences between peaks diminish with further increases in groundwater levels. Again, clay shows consistently lower peak velocities compared to sand, reinforcing the impact of soil permeability on hydrogen leakage dynamics.

These observations highlight that while the immediate boundary conditions primarily determine leakage rates, factors such as pipe depth and groundwater levels significantly affect the broader dispersion and velocity of hydrogen as it moves through the soil and reaches the atmosphere.

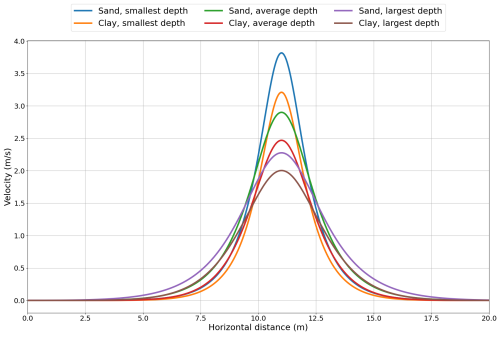

(a) Velocity profile at the boundary between soil and atmosphere with different pipe depths for MG and leak size of 1 cm.

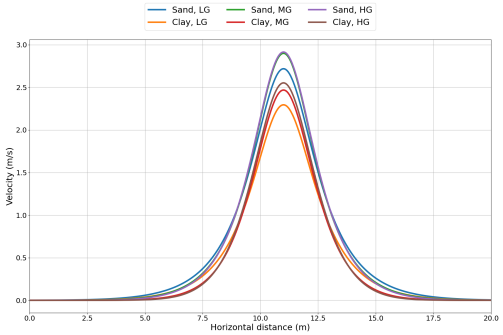

(b) Velocity profile at the boundary between soil and atmosphere with different groundwater levels for average pipe depth and leak size of 1 cm.

Figure 4.8: Impact of pipe depth and groundwater level on hydrogen velocity profiles at the boundary between soil and atmosphere.

4.5 Sand vs Clay

Figure 4.9 shows the difference in hydrogen leaked as a function of soil type for the hole sizes. Figure 4.9a shows the percentage of hydrogen leaked for the sand and clay when the pipe is at its smallest depth and the groundwater level is LG. It shows that the percentage

of hydrogen leaked is almost identical. Figure 4.9b shows the percentage of hydrogen leaked for sand and clay when the pipe is at its largest depth and the groundwater level is HG. It shows that there is relatively more leakage in sandy soil, especially in the larger hole scenarios. This difference can be as large as two %-points. This result shows that the type of soil does influence the percentage leaked, this difference is relatively small. In addition, it was found that sand consistently leaks more hydrogen compared to clay.

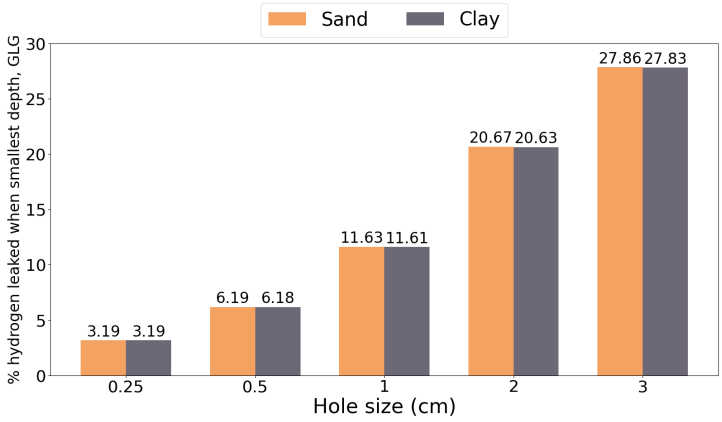

(a) Smallest pipe depth and LG groundwater level

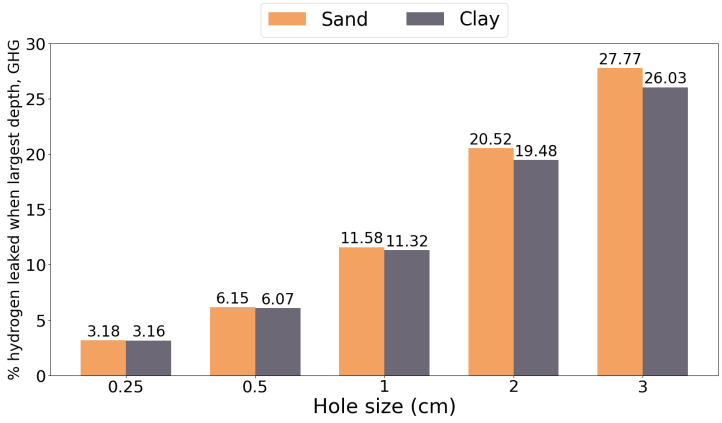

(b) Largest pipe depth and HG groundwater level

Figure 4.9: The percentage of hydrogen leaked in clay for different depths of pipes and groundwater levels.

The differences in the permeability and density of the soils can explain this disparity in leakage rates. Sand has a higher permeability than clay, allowing hydrogen to flow more readily. The permeability is calculated with equation 3.24 with d_p equal to 0.5 mm

and 0.05 mm and ϵ_p equal to 0.25 and 0.43, for sand and clay respectively [23]. The resulting permeability is then equal to $4.6 \cdot 10^{-5}$ m^2 and $4.078 \cdot 10^{-6}$ m^2 for sand and clay respectively. Additionally, clay has a higher density, leading to a greater pressure exerted by the soil on the pipeline. Consequently, the combination of lower permeability and higher density in clay leads to reduced hydrogen leakage compared to sand under the same conditions.

In scenarios where the pipeline is submerged, the difference in leakage rates between sand and clay is even more pronounced. This increase in disparity can be explained by the difference in the relative permeability factor of sand and clay. The relative permeability factor, which is used in calculating the permeability of the saturated soil (equation 3.25, is five times lower for clay than for sand (0.01 [65] versus 0.05 [63; 64] respectively). Consequently, when the pipeline is submerged under water, clay will have a permeability that is five times smaller than sand. This lower permeability of clay significantly restricts the flow of hydrogen, thereby reducing the leakage compared to sand. This effect is apparent in the figures, where submerged conditions consistently show a more pronounced difference in leakage between the two soil types.

Interestingly, the results also show that the difference in hydrogen leakage between sand and clay increases as the hole size in the pipeline increases. This relationship is particularly noticeable in the larger hole sizes, where the percentage of hydrogen leaked is higher overall.

The increase in the difference between sand and clay leakage rates with increasing hole size can be explained by considering the interaction between the flow rate of hydrogen through the hole and the permeability of the surrounding soil. As the hole size increases, the rate of hydrogen escaping from the pipeline also increases. In sand, which has a higher permeability, this increased flow rate can be more readily accommodated, resulting in a larger volume of hydrogen being lost to the environment. In contrast, the lower permeability of clay acts as a bottleneck, restricting the flow and thereby reducing the amount of hydrogen that can escape. The key point is that as the hole size increases, the flow rate through the hole increases disproportionately in sand due to its higher permeability. This larger increase in flow rate leads to a more pronounced difference in leakage between sand and clay as the hole size increases, thereby amplifying the observed difference in leakage percentages between the two soil types [114].

These phenomena can also be seen in the larger pressure build-up at the hole boundary in clay compared to sand. Figure 4.10 shows the pressure profile in sand and clay at the hole boundary for the following scenarios and hole sizes: Figures 4.10a and 4.10b shows the largest depth of pipe with the highest groundwater level for a hole size of 0.25 cm and 3 cm, Figure 4.10c shows the smallest depth of the pipe with the lowest groundwater level for a hole size of 3 cm. Figure 4.10c shows the small pressure difference built up at the hole boundary for clay and sand. This difference is due to clay's higher density and lower permeability than sand. However, the difference is relatively small. This can also be seen when looking at the leakage rate in Figure 4.9a. The difference becomes much more noticeable when a saturated layer of soil is added. In Figures 4.10a and 4.10b

can be seen how there is much more pressure build-up in the clay soil compared to the sand soil. This can also be seen in the bigger difference in leakage rat in Figure 4.9b. This corroborates the explanation behind the decreased leakage rate in clay compared to sand. Additionally, it shows that the pressure difference increases for an increase in hole size (129% increase in average pressure for a hole size of 0.25 cm and 213% increase in average pressure for a hole size of 3 cm), corroborating the results showing that the disparity between the leakage rates increases for an increase in hole size.

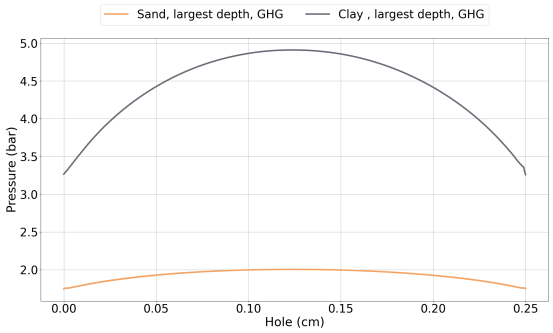

(a) Largest depth of the pipe and highest groundwater lever with a hole size of 0.25 cm

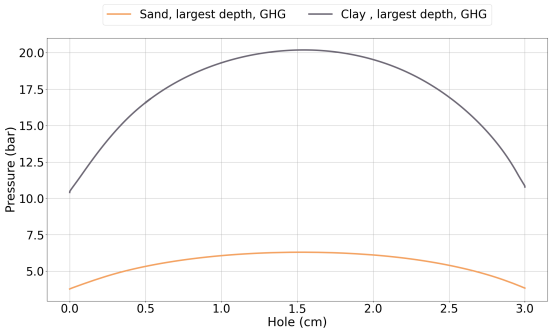

(b) Largest depth of the pipe and highest groundwater lever with a hole size of 3 cm

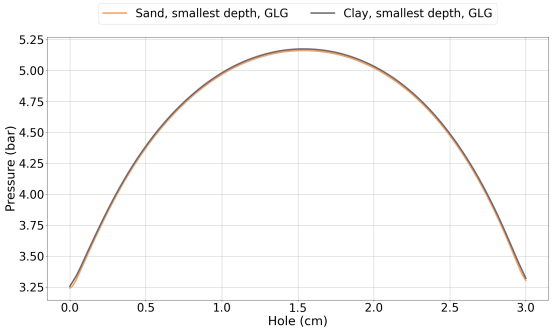

(c) Lowest depth of the pipe and lowest groundwater lever with a hole size of 3 cm

Figure 4.10: The pressure profile at the boundary of the hole for different scenarios

4.6 Safety Risk

Figure 4.11 shows the horizontal dispersion of hydrogen measured from the centre of the hole to where the leakage rate into the atmosphere is equal to 0.5 m/s. The different subplots show the dispersion per hole size for sand vs clay and different parameters such as pipe depth and groundwater level.

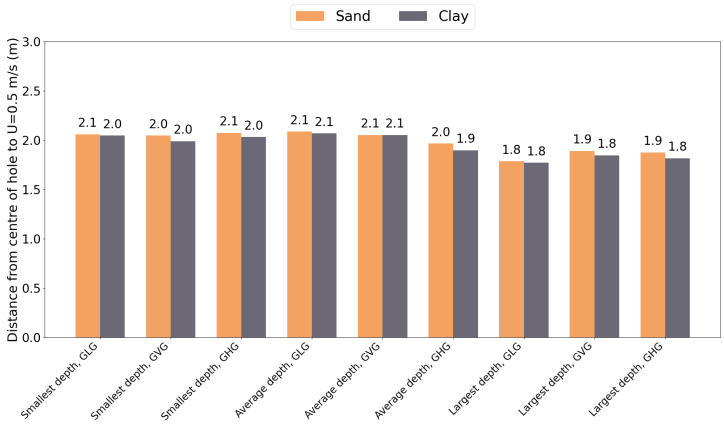

(a) Hole size 0.25 cm

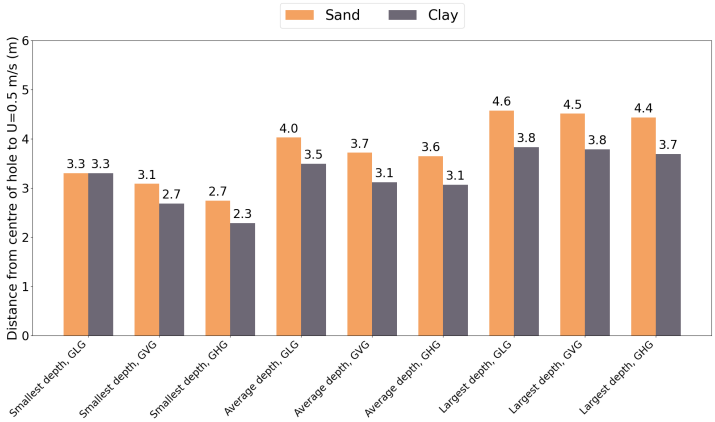

(b) Hole size 3 cm

Figure 4.11: The horizontal dispersion of hydrogen measured from the centre of the hole to the point where the velocity reaches 0.5 m/s

As can be seen in these figures, the horizontal range of hydrogen dispersion increases with soil depth. This trend is consistent for both sand and clay and can be explained by the increased distance the hydrogen must travel before reaching the surface, allowing for greater lateral diffusion.

Conversely, an increase in groundwater level results in a reduction of the horizontal range, observable in all figures. This effect is more pronounced in clay than in sand, reflecting the higher resistance to gas flow presented by clay's lower permeability when saturated. In soils with higher water content, the hydrogen gas encounters greater resistance as it diffuses through the pore spaces, which reduces its lateral spread.

The comparison between sand and clay further emphasizes the impact of soil type on hydrogen dispersion. Across all depths and water levels, clay consistently exhibits a

shorter range compared to sand. This is due to the inherently lower permeability and higher density of clay, which impede the movement of gas more effectively than sand. In most cases, the difference in range between sand and clay is most significant at the highest water level, underscoring the compound effect of reduced permeability in clay combined with the resistance posed by increased water saturation.

These findings suggest that soil type, depth, and groundwater levels are critical factors in determining the extent of hydrogen dispersion. In scenarios where hydrogen leakage occurs in areas with higher clay content and increased water saturation, the expected horizontal dispersion range will be significantly lower than in sandy soils, impacting the safety considerations for hydrogen infrastructure.

Interestingly, as illustrated in Figure 4.11a, when the hole size is reduced to 0.25 cm, the distinction between the range and the pipe depth becomes negligible. This phenomenon can be better understood by examining the velocity profile at the boundary to the atmosphere for different scenarios, as depicted in Figure 4.12. The figure shows the velocity at the boundary to the atmosphere for a hole size of 0.25 cm and a groundwater level of MG.

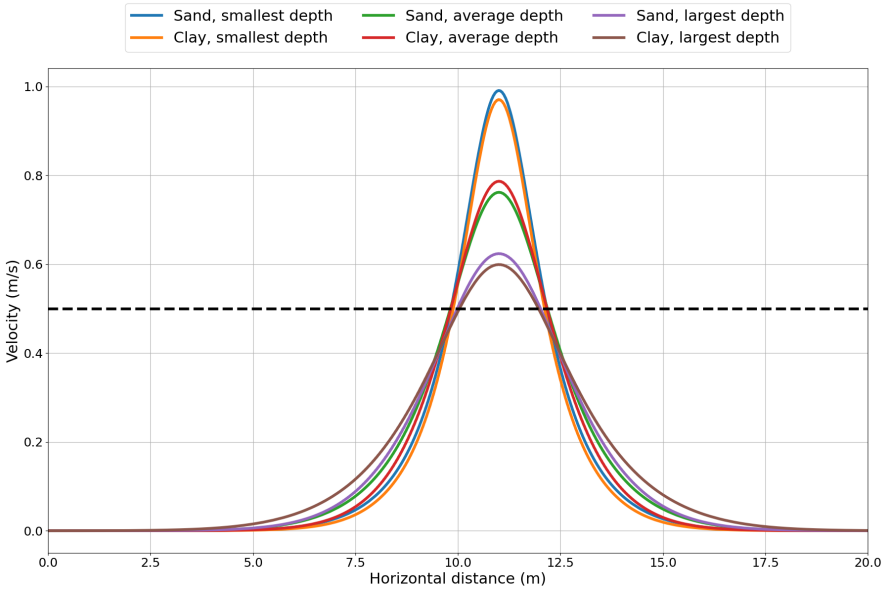

Figure 4.12: Velocity profile at the boundary to the atmosphere for a hole size of 0.25 cm and groundwater level MG

The velocity profile reveals that although there is a wider spread when the pipe depth increases, the velocity at the boundary remains relatively low. Consequently, the cutoff velocity of 0.5 m/s is reached before the peak velocities at lower depths decrease sufficiently to be "caught" by the wider spread but lower peak velocities at larger depths. This results in a situation where the horizontal range of hydrogen dispersion decreases for increased pipe depth.

Figure 4.11 shows that the maximum horizontal dispersion is approximately 4.5 m. This would indicate that there should be a minimum safe zone of 4.5 m around the pipelines to ensure that there is no risk of a hydrogen fire. This corresponds with the Dutch regulations for gas pipelines which range between 4 and 50 meters depending on the diameter and pressure of the pipeline [22]. However, it is important to keep in mind that in this research only a leak on the top of the pipe was taken into account. If the leak would be on the side, due to the high-pressure difference, this range would likely be much higher. Therefore, this number only serves as a minimum indication of a safety distance.

4.7 Monte Carlo Analysis

The Monte Carlo analysis yielded a probabilistic distribution of the percentage of hydrogen leaked from the pipeline under various scenarios. The results provide valuable insights into the expected leakage behaviour and the associated uncertainties.

The probability distribution of the percentage of hydrogen leaked, as illustrated in Figure 4.13, shows a strong right-skewness with a significant concentration of lower leakage values. Key statistical measures from the analysis include a mean leakage of 0.06%, and a P_{95} leakage of 0.18%. These values indicate that most leakage events, when the assumption of 1 leakage per year is valid, are likely to be minimal. The sudden drop at approximately 0.12% is due to the switch from the immediate detected leaks to the non-immediate detected leaks, since the immediate detected leaks can not leak more than 0.12% when there is only 1 leak per year and the maximum detection time is 12 hours.

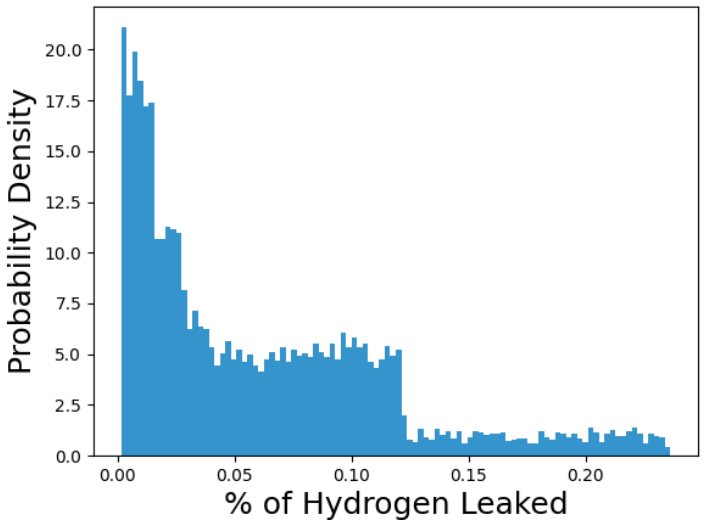

Figure 4.13: Probability distribution of the percentage of hydrogen leaked per year found from the Monte Carlo analysis

The distribution reflects the high uncertainty and variability in the system parameters, particularly in the size of leaks and the duration of leakage events. The sharp peak near zero suggests that in many simulations, the percentage of hydrogen leaked was minimal, likely due to the small number of leaks and relatively short leakage time. However, the long tail extending towards higher percentages indicates that there are scenarios where the leakage could be more significant.

In summary, the Monte Carlo analysis reveals that the majority of hydrogen leakage events are expected to be minor, with a mean leakage of 0.06% and a strong right-skewed distribution indicating higher probabilities for low leakage rates. The analysis highlights the inherent uncertainties and variability in leakage scenarios, emphasizing the importance of understanding both the frequency and size of leaks to better predict and mitigate potential hydrogen losses.

4.7.1 Environmental Impact

The potential environmental impact of hydrogen leakage was assessed by calculating the total amount of hydrogen that could be leaked under two different scenarios: the expected hydrogen usage in 2030 (100 PJ [13]) and the hypothetical scenario where hydrogen completely replaces natural gas in the Netherlands (997.096 PJ [73]). The results of these scenarios, expressed in kilotonnes (kTonnes) of hydrogen leaked, are illustrated in Figure 4.14.

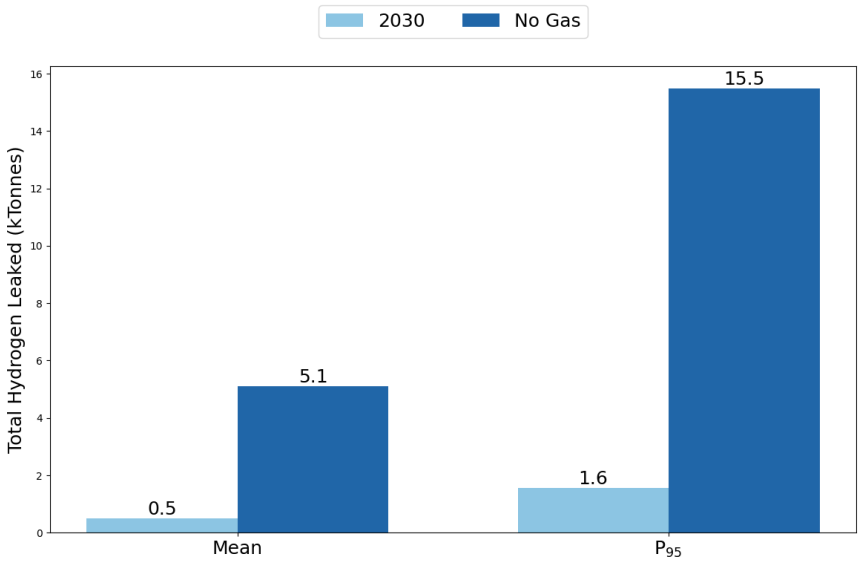

Figure 4.14: Total MTonnes of Hydrogen Leaked for the 2030 and Complete Natural Gas Replacement Scenarios.

As shown in Figure 4.14, the Monte Carlo analysis indicates that the amount of hydrogen

leaked could vary significantly between the scenarios. For the 2030 scenario, the mean leakage is projected to be relatively low, around 0.5 kTonnes, while the P_{95} reaches approximately 1.6 kTonnes. In contrast, the complete substitution of natural gas with hydrogen results in a much higher mean leakage of around 5.1 kTonnes, with the P_{95} reaching up to 15.5 kTonnes, which is a factor 10 higher. These results underscore the substantial increase in hydrogen leakage associated with larger-scale hydrogen deployment.

To understand the environmental implications, the leaked hydrogen was converted into CO_2-equivalent emissions using a GWP100 of 16.5, as found by Ocko and Hamburg [44]. The resulting CO_2-eq emissions for the hydrogen leakage are compared to the current CO_2-eq emissions from natural gas in the Netherlands in Figure 4.15.

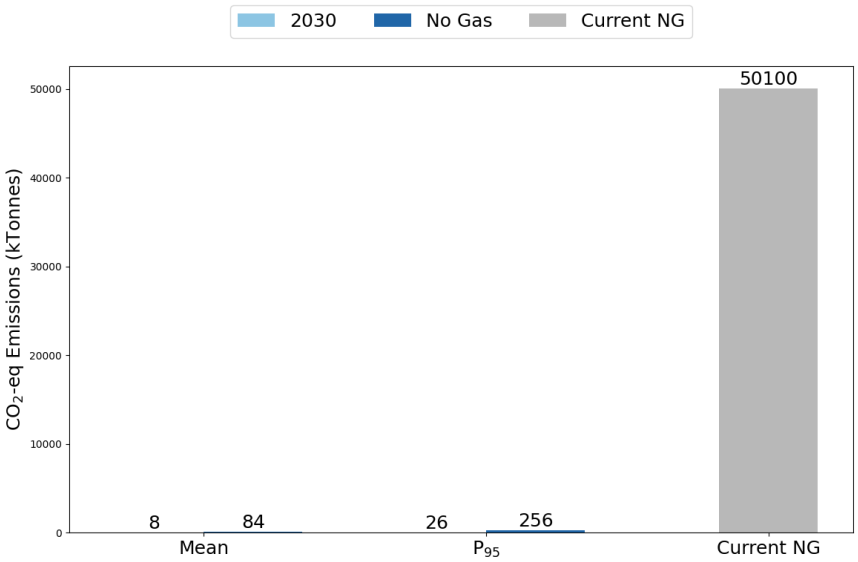

Figure 4.15: CO_2-eq Emissions (kTonnes) from Hydrogen Leakage Compared to Current Natural Gas Emissions in the Netherlands.

Figure 4.15 illustrates that in the 2030 scenario, the mean CO_2-eq emissions from hydrogen leakage are relatively low, ranging from 8 to 26 kTonnes. Even in the complete replacement scenario, where emissions are higher, the P_{95} reaches only 256 kTonnes. This is still approximately 200 times lower than the current CO_2-eq emissions from natural gas, which are estimated to be around 50,100 kTonnes. These results suggest that, from an environmental perspective, hydrogen leakage from high-pressure pipelines poses minimal risk and offers a substantial reduction in greenhouse gas emissions compared to natural gas usage. Even in the worst-case scenario, hydrogen leakage would result in significantly lower emissions, highlighting the environmental benefits of transitioning to hydrogen as an energy source.

However, the data also highlight a critical point: the environmental benefits of switching

to hydrogen are heavily dependent on controlling the number of leaks per year and the leakage time. Due to the GWP100 of hydrogen, even small leaks can lead to non-negligible greenhouse gas emissions. For instance, Figure 4.7a shows that a hole with a diameter of just 0.25 cm can result in leakage rates of up to 3%. This reinforces the need for strict monitoring and mitigation strategies to minimize leakage throughout the hydrogen supply chain, ensuring that the transition to hydrogen does indeed lead to a substantial reduction in overall greenhouse gas emissions.

In conclusion, the Monte Carlo analysis indicates that hydrogen leakage from high-pressure pipelines, even in the worst-case scenarios, results in significantly lower CO_2-equivalent emissions compared to current natural gas usage. However, to fully realize these environmental benefits, it is vital to implement effective leak detection, monitoring, and mitigation strategies that can control the number and duration of leaks.

4.7.2 Financial Impact

The financial impact of hydrogen leakage was evaluated by considering the projected price of hydrogen for the two previously mentioned scenarios. This part of the Monte Carlo analysis incorporated variability in hydrogen prices across different types (grey, blue, and green hydrogen) as well as the variability in hydrogen leakages, leading to a probabilistic distribution of potential financial losses due to leakage.

The probability distributions of financial losses for both scenarios are presented in Figure 4.16. These figures show the wide range of potential financial losses, with a clear right-skewness, indicating that while most scenarios result in relatively low financial losses, there are significant outliers where losses could be much higher.

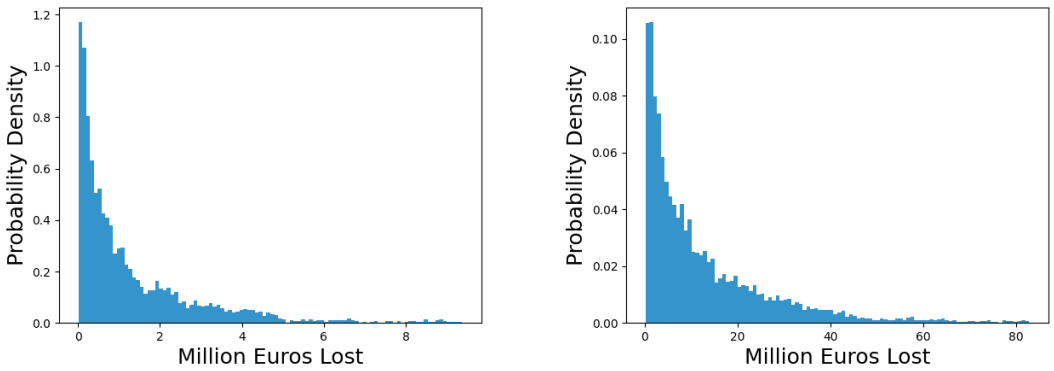

(a) 2030 Scenario *(b) No Gas Scenario*

Figure 4.16: Probability Distribution of Euros lost

Figure 4.16a illustrates the potential financial losses in the 2030 scenario, the sharp peak near zero suggests that in many simulations the financial loss is minor. However, the long

tail of the distribution shows that there is a non-negligible risk of significantly higher losses. This pattern is also present in the No Gas scenario (Figure 4.16b).

To compare the financial losses across the scenarios more clearly, the mean, and P_{95} values are shown in Figure 4.17. The figure highlights the stark difference between the 2030 and No Gas scenarios. In the 2030 scenario, the mean financial loss is approximately 1.3 million euros, with the P_{95} at approximately 4.5 million euros. In contrast, the No Gas scenario shows a mean loss of about 12.4 million euros, with a P_{95} loss of nearly 41 million euros. In comparison, these potential losses in the worst-case scenario amount to nearly 10% of Gasunie's net profit of 483.3 million euros reported in the year 2023 [115].

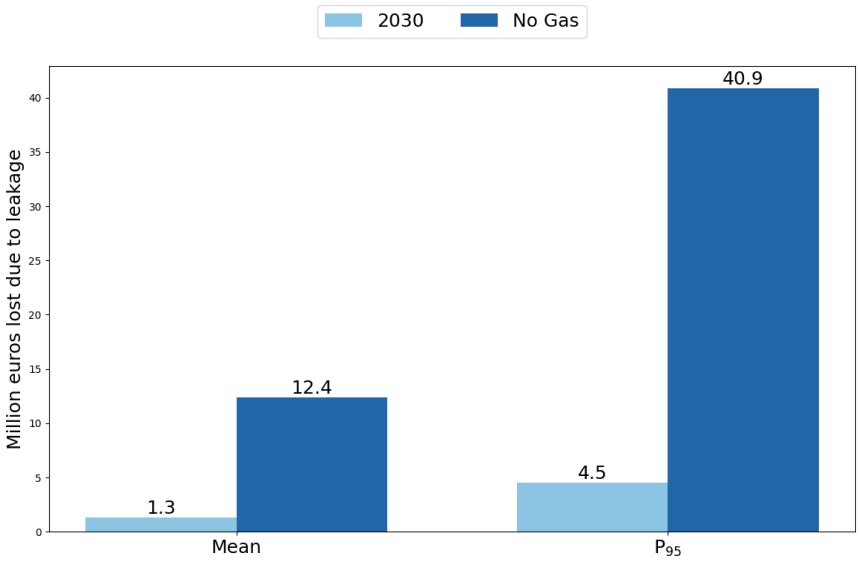

Figure 4.17: Euros Lost Due to Hydrogen Leakage.

These results underscore the financial risks associated with hydrogen leakage, especially as hydrogen deployment scales up. The significant increase in potential losses in the No Gas scenario reflects the larger volumes of hydrogen involved and the higher associated costs. It is also important to note that these financial risks are influenced not only by the volume of hydrogen leaked but also by the price volatility of hydrogen, particularly for green hydrogen, which is expected to constitute a larger share of the hydrogen mix by 2050 [70; 71].

In conclusion, while the financial impact of hydrogen leakage in the 2030 scenario is expected to be relatively manageable, the risks become much more pronounced in scenarios involving large-scale hydrogen deployment. These findings highlight the importance of robust leak detection and prevention strategies to mitigate the financial risks associated with hydrogen leakage. Additionally, the variability in hydrogen prices suggests that

market conditions will play a significant role in determining the ultimate financial impact of hydrogen leakage.

4.8 Sensitivity Analysis

The sensitivity analysis on the Monte Carlo model reveals a consistent linear relationship between the expected number of leaks per year and the associated outcomes, as shown in Figures 4.18a through 4.18d. This linearity was expected, as more leaks per year directly increase the volume of hydrogen escaping from the system, leading to higher financial losses and greater environmental impact.

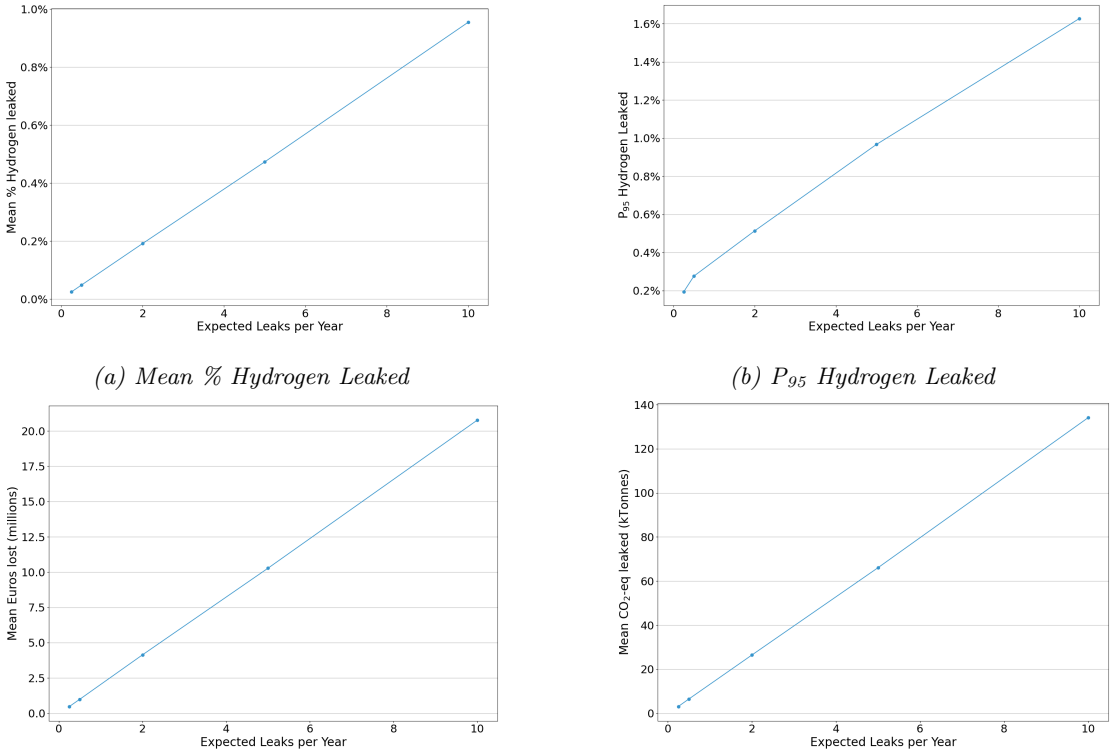

(a) Mean % Hydrogen Leaked

(b) P_{95} Hydrogen Leaked

(c) Mean Euros Lost

(d) Mean CO_2-eq Emitted

Figure 4.18: Sensitivity Analysis Results: Impact of Expected Number of Leaks Per Year on Mean % Hydrogen Leaked, P_{95} Hydrogen Leaked, Mean Euros Lost, and Mean CO_2-eq Emitted for the 2030 Scenario.

The mean percentage of hydrogen leaked (Figure 4.18a) and the P_{95} of hydrogen leakage (Figure 4.18b) both increase proportionally with the number of leaks, reaching nearly 1% and over 1.6%, respectively, with 10 expected leaks per year. These results highlight the significant impact of leak frequency on hydrogen loss, which is particularly concerning given hydrogen's propensity to leak due to its smaller molecular size compared to natural gas [74; 21], so there could be more hydrogen leakages than the 1 per year assumed in

this research.

In the 2030 scenario, both mean financial losses (Figure 4.18c) and mean CO_2-eq emissions (Figure 4.18d) increase linearly with the number of leaks. Financial losses range from approximately 0.25 million euros for a quarter of a leak per year to nearly 20 million euros for ten leaks per year, while CO_2-eq emissions rise from under 5 kTonnes to over 120 kTonnes. Although these emissions remain lower than those from natural gas, they still present a notable environmental impact, considering hydrogen's greenhouse gas potential.

These findings emphasize the substantial economic and environmental risks associated with increased leak frequency in hydrogen pipelines. The higher likelihood of leaks due to hydrogen's smaller molecular size compared to natural gas makes robust leak detection and mitigation strategies essential to ensuring the sustainability and safety of hydrogen as a key energy carrier in future energy systems.

The sensitivity analysis in Figures 4.19a through 4.19d evaluates the impact of varying immediate and non-immediate detection times, the ratio of immediate to non-immediate detection, and the leak rate which gets detected immediately on the percentage of hydrogen leaked, financial losses, and CO_2-equivalent emissions. The results show that non-immediate detection time and leak rate that gets detected immediately have the most significant influence on the mean percentage of hydrogen leaked and the P_{95} of hydrogen leaked.

The parameter for the immediate detected leak rate increases in discrete steps. This behavior is because the leak rates considered in this study correspond to five leak sizes, which each have a roughly similar leakage rate. Consequently, if the immediate detected leak rate changes but does not surpass the threshold of another defined leak size, the amount of hydrogen leaked remains relatively stable, except for variations introduced by different scenarios and randomness from the Monte Carlo analysis. However, when a threshold is crossed, such as when a smaller leak is detected immediately, there is a noticeable sharp decrease or increase in the percentage of hydrogen leaked.

As the non-immediate detection time increases, the associated metrics exhibit a linear increase, indicating that the duration before a leakage is detected using intermittent methods is a critical risk factor in hydrogen leakage scenarios. This finding highlights that the non-immediate detection time, alongside the capability to detect smaller leaks immediately, is among the most influential parameters affecting hydrogen leakage outcomes.

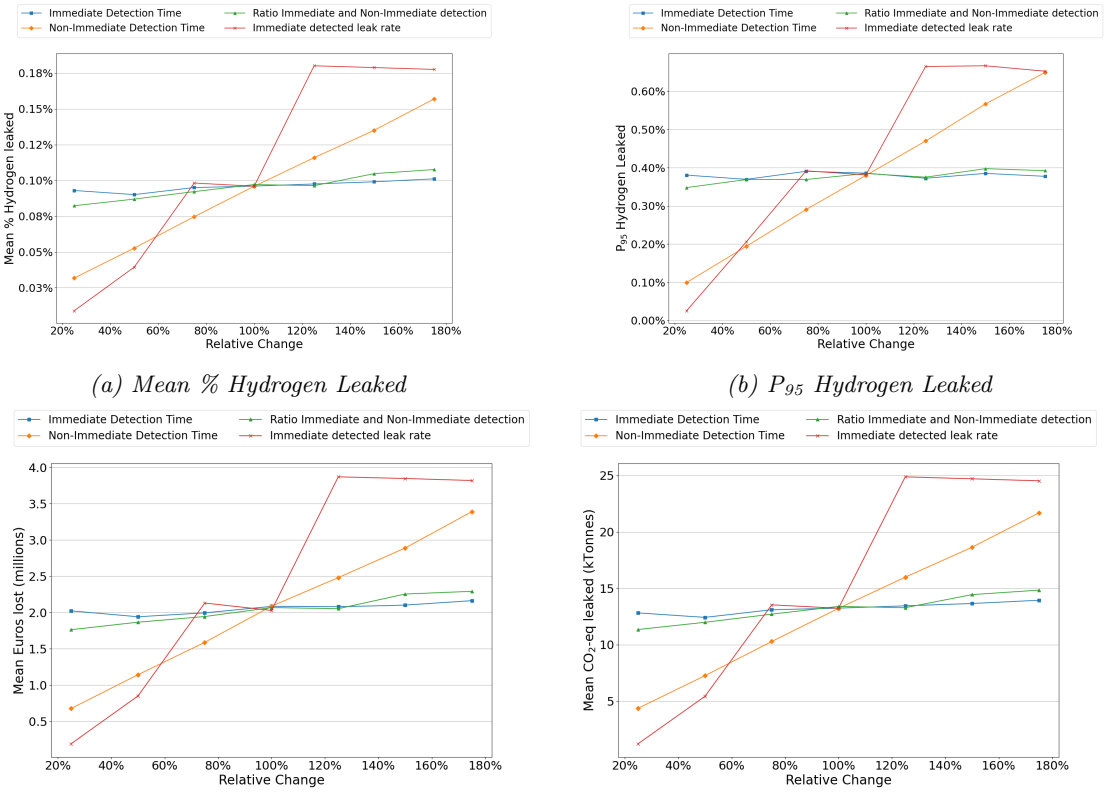

(a) Mean % Hydrogen Leaked

(b) P_{95} Hydrogen Leaked

(c) Mean Euros Lost

(d) Mean CO_2-eq Emitted

Figure 4.19: Sensitivity Analysis Results: Impact of Detection Times and Ratios on Mean % Hydrogen Leaked, P_{95} Hydrogen Leaked, Mean Euros Lost, and Mean CO_2-eq Emitted for the 2030 Scenario.

By contrast, variations in immediate detection time and the ratio of immediate to non-immediate detection have a smaller impact on these outcomes. This suggests that while immediate detection is essential, the precise duration taken to address a leak (e.g., 2 hours versus 24 hours) has a less significant effect on the overall leakage. Consequently, prioritizing technologies that consistently detect even small leaks, despite not being able to pinpoint their exact location, could be more effective in minimizing financial and environmental consequences.

These findings advocate for regular intermittent detection methods, particularly in the initial stages of pipeline operation, to minimize the risks associated with undetected leaks. Consistent and frequent monitoring can significantly reduce detection times, limiting hydrogen leakage and its associated impacts. Moreover, favouring detection technologies that can identify small leaks, even without precise localization, over those that only detect larger leaks with high accuracy, could offer a more balanced approach to mitigating financial losses and environmental damage.

5 Conclusion

The primary research question of this study was:

What are the environmental, financial, and safety-related risks of transporting hydrogen through underground natural gas pipelines?

The results show that the environmental impact of hydrogen leakage in terms of CO_2-eq is small, especially when compared to the current emissions from natural gas. The financial implications, on the contrary, could be substantial. This is based on leak sizes that range from 0.25 - 3 cm, an occurrence of one leak per year, and no multiple leak points at the same time. Regarding the safety-related risks, the flammability risk and the subsequent safety range that should be implemented is relatively small being 4.5 m.

The percentage of leaked hydrogen varies significantly with the leak size. For instance, as shown in Figure 4.6, a hole size of 0.25 cm results in a leakage of 3.2% of the total hydrogen transported, depending on soil type and pipeline depth. As the hole size increases, the leakage percentage rises sharply, reaching up to 27% for a hole size of 3 cm in some scenarios.

The influence of groundwater level and depth of pipe on the leakage rate is small but noticeable, while the influence of the soil type is larger but still relatively small. Specifically, deeper pipelines and higher groundwater levels tend to reduce the percentage of hydrogen leaked. However, this reduction is relatively small compared to the influence of hole size. As depicted in Figures 4.6 and 4.7, the difference in leakage percentages between the smallest and largest pipeline depths is less than 1%-point across most scenarios. As seen in Figure 4.9, the difference between sand and clay can increase to 2%-point, with more hydrogen leakage observed in sand than in clay due to its higher permeability.

However, the pipe depth and groundwater level do have an impact on the dispersion of hydrogen through the soil, as shown by the velocity profiles (Figures 4.8a and 4.8b). These factors influence the spread of hydrogen and its subsequent release into the atmosphere, which carries significant safety implications. Although they may not change the leakage rates measured at the pipe-soil boundary, they are important considerations in scenarios involving potential reactions between hydrogen and soil microorganisms.

Hydrogen leakages from high-pressure underground pipelines have an environmental impact but this is much lower than the current emissions from natural gas. For example, in the scenario where hydrogen completely replaces natural gas, even the P_{95} of CO_2-eq emissions due to hydrogen leakage (256 kTonnes) is still much lower than the current 50,100 kTonnes of CO_2-eq emissions from natural gas. This indicates that hydrogen leakage in high-pressure pipelines poses a much smaller risk for the environment compared to continued natural gas usage, as long as leaks are minimized.

The financial impact of hydrogen leaks can be considerable, especially in

scenarios involving large-scale hydrogen deployment. As shown in Figures 4.16 and 4.17, the financial loss due to hydrogen leakage can reach up to 41 million euros in the scenario where hydrogen replaces natural gas completely. This is approximately 10% of the total net profit of Gasunie from 2023. This underscores the importance of robust leakage detection and prevention strategies to mitigate financial risks.

There should be a minimum safety zone of 4.5 meters around the pipelines to ensure no risk of a hydrogen-fueled fire. This is based on the maximum horizontal dispersion observed in the simulations (Figure 4.11). However, it is important to note that this number serves as a minimum safety distance, as only leaks on the top of the pipe were considered. Leaks on the side of the pipe, larger leak sizes, and multiple leaks near each other could require a larger safety zone.

The sensitivity analysis shows that the number of leaks per year, the immediate detected leak rate, and the non-immediate detection time are the most significant factors influencing the financial and environmental impact of hydrogen leakage. The immediate detected leak rate plays a significant role, specifically when the leak rate of smaller hole sizes is detected immediately it causes the biggest decrease in hydrogen leaked. A linear relationship was observed between the leak frequency and key outcomes such as hydrogen loss, financial losses, and CO_2-eq emissions. Although immediate detection time and the ratio of immediate to non-immediate detection have relatively smaller impacts, they still contribute to overall risk mitigation. Implementing regular intermittent detection and investing in technologies that can consistently identify even small leaks, irrespective of their precise location, are essential strategies for effectively managing the risks associated with hydrogen transport.

There is a wide range of leakage detection methods. Each method has its upsides and downsides, making the choice dependent on specific pipeline requirements such as real-time monitoring, cost, and accuracy in leak detection and location. Selecting the most suitable method often involves balancing these factors. For optimal protection, combining multiple detection techniques can be effective, as this approach utilizes the complementary strengths of each method.

In summary, this research provided a comprehensive evaluation of the risks associated with hydrogen leakage in repurposed high-pressure natural gas pipelines. While the environmental impact and the flammability risk are relatively small, the financial impact could be substantial, particularly in large-scale hydrogen deployment scenarios. These findings emphasize the critical need for effective monitoring, leakage detection, and prevention strategies to ensure the safe and economically viable transportation of hydrogen within the transmission network.

6 Future Outlook

This research has highlighted several areas in which uncertainties about the risks of hydrogen leakages exist. This section discusses the future outlook for research and practical measures that should be undertaken to address the challenges identified. One general point is to account for the entire hydrogen supply chain instead of only the high-pressure hydrogen pipelines. This will give a more inclusive view of the potential environmental and financial impact.

Simulation Expansion
The current study has primarily focused on two-dimensional simulations, which have limitations in capturing the full complexity of hydrogen leakage and diffusion in real-world conditions. Expanding the simulation framework to include three-dimensional models will allow for a more detailed understanding of the leak dynamics and their interaction with the surrounding environment.

Interesting research directions could be assessing the impact of various soil deformations and potential crater formations around the leak site, which could significantly alter the leakage rate and dispersion patterns.

Additionally, the simulations should consider scenarios where the leak occurs on different sides of the pipe rather than on top, as this could affect the safety distance required around the pipeline. Cross-referencing these scenarios with the locations of industrial and residential areas near the hydrogen backbone could be used to identify potential danger zones.

Future simulations should also account for the effects of different climate conditions, such as seasonal temperature variations, freezing and thawing cycles, and extreme weather events, on hydrogen leakage rates and pipeline integrity. Climate conditions can significantly impact soil properties, such as permeability and porosity, as well as the physical integrity of pipelines.

In this study, a limited scenario analysis was conducted, with five distinct hole sizes and one set pressure level and flow rate. Future work should include a broader range of leak sizes and varying pipeline pressures and flow speeds. By doing so, a more comprehensive dataset can be built. In practical applications, the pressure at different points of the pipe will also differ and the flow rate will depend on the demand.

This research focused on the hydrogen dispersion through the soil and determined a safety range from this. To enhance the safety of hydrogen transportation, it is recommended that future simulations also examine the dispersion of hydrogen through the air. This will provide better information to inform safety regulations, particularly in estimating the safety zone from the pipelines to industrial and residential areas. Simulating the time required for the system to reach a steady state post-leak could also give insightful information about the system.

Experimental Validation and Data Collection
The results of this study are based on simulations. While valuable, more practical experimental data is necessary to verify the results. Experimental data will provide deeper insights into the system's proneness to leak and offer practical confirmation of the simulation results. This empirical data is crucial to validate the model's predictions and refine its accuracy, particularly in complex scenarios that involve variable soil types, groundwater levels, and other environmental factors. Moreover, more comprehensive data on soil properties such as permeability, porosity, and their correlation with groundwater levels that can be obtained through experiments are essential for enhancing the precision of future simulations.

The mentioned scenario in the simulation expansion section should also be included in experiments. A key missing element in the literature is the missing empirical data on hydrogen leakages in various scenarios.

Environmental Impact
This study briefly touched on the role of microbial hydrogen consumption. However, while this was identified as having a potentially significant impact on hydrogen losses, it was not fully explored in this study. Future work should investigate whether microbial consumption could meaningfully reduce hydrogen leakage and its associated environmental impacts.

In this study, the environmental focus was primarily on CO_2-equivalent emissions, but other environmental metrics such as soil quality are also important to take into account. Understanding how hydrogen leakages and hydrogen-soil interactions affect these factors is necessary to gain a complete view of the environmental consequences of hydrogen leakage and ensure sustainable hydrogen deployment.

Detection Methods
In this research, a range of hydrogen leakage detection methods was briefly discussed (subsection 4.2. The results from subsection 4.7 highlight the importance of implementing effective detection techniques to mitigate both financial and environmental risks associated with hydrogen leaks. In this study, assumptions were made on the effectiveness of detection methods. Gathering real-world data on which detection systems and their performances utilized by Gasunie could add to the credibility of the results.

Researching proper leak detection and location techniques is essential not only for immediate leak identification but also for building a comprehensive database of leakage incidents. Such a database can provide valuable insights for developing long-term prevention strategies.

Future research should focus on testing the accuracy and reliability of the detection techniques to ensure their effectiveness in identifying specifically hydrogen leaks. This should include evaluating both technological innovations in detection equipment and computational methods for early leak identification. Additionally, exploring different

combinations of detection methods to determine the most effective and economically viable solutions is important to ensure practical applications.

Hydrogen Supply Chain
This research focused specifically on the repurposed high-pressure gas pipelines. To get a complete insight into the risks associated with large-scale hydrogen deployment, the entire supply chain should be taken into account. Currently, in literature, only assumptions are made of the leakage during the production, transportation, and utilization. This should be modeled properly to get a complete view of the hydrogen leakages in the whole system.

Finally, future research should consider comparing the risks and benefits of hydrogen transport through pipelines with alternative energy storage and transport solutions, such as ammonia or liquid organic hydrogen carriers (LOHCs). Understanding these technologies' relative advantages and disadvantages can provide a more comprehensive perspective on the best strategies for hydrogen transport within the broader context of the energy transition.

This research provides valuable insights into the risks associated with hydrogen leakage in repurposed high-pressure natural gas pipelines. However, it serves as a stepping stone toward more research needed to understand the risks associated with large-scale hydrogen utilization fully. Future research should focus on several critical areas: gathering empirical data on hydrogen leakages to improve our understanding of leakage behavior, analyzing the entire hydrogen supply chain to quantify leakages at each stage, conducting 3D simulations that account for soil deformation, and investigating other environmental impacts of hydrogen leakage, such as effects on soil quality.

References

[1] Ministerie van Economische Zaken en Klimaat. Klimaatakkoord - Klimaatakkoord, 3 2023. URL https://www.klimaatakkoord.nl/.

[2] Netbeheer Nederland. Capaciteitskaart invoeding elektriciteitsnet, 2023. URL https://capaciteitskaart.netbeheernederland.nl/.

[3] Johan Ehlers, Anders A. Feidenhans'l, Kasper T. Therkildsen, and Gastón O. Larrazábal. Affordable Green Hydrogen from Alkaline Water Electrolysis: Key Research Needs from an Industrial Perspective. *ACS Energy Letters*, 8(3):1502–1509, 2 2023. doi: 10.1021/acsenergylett.2c02897. URL https://doi.org/10.1021/acsenergylett.2c02897.

[4] Seyed Ehsan Hosseini and Mazlan Abdul Wahid. Hydrogen from solar energy, a clean energy carrier from a sustainable source of energy. *International Journal of Energy Research*, 44(6):4110–4131, 5 2020. doi: 10.1002/er.4930. URL https://doi.org/10.1002/er.4930.

[5] Lei Zhang, Cunqi Jia, Fuqiao Bai, Wensen Wang, Senyou An, Kaiyin Zhao, Zihao Li, Jingjing Li, and Hai Sun. A comprehensive review of the promising clean energy carrier: Hydrogen production, transportation, storage, and utilization (HPTSU) technologies. *Fuel*, 355:129455, 1 2024. doi: 10.1016/j.fuel.2023.129455. URL https://www.sciencedirect.com/science/article/pii/S0016236123020690.

[6] Alessandro Cappelletti and Francesco Martelli. Investigation of a pure hydrogen fueled gas turbine burner. *International Journal of Hydrogen Energy*, 42(15):10513–10523, 4 2017. doi: 10.1016/j.ijhydene.2017.02.104. URL https://www.sciencedirect.com/science/article/pii/S0360319917306122.

[7] Michele Stefanizzi, Tommaso Capurso, Giovanni Filomeno, Marco Torresi, and Giuseppe Pascazio. Recent Combustion Strategies in Gas Turbines for Propulsion and Power Generation toward a Zero-Emissions Future: Fuels, Burners, and Combustion Techniques. *Energies*, 14(20):6694, 10 2021. doi: 10.3390/en14206694. URL https://www.mdpi.com/1996-1073/14/20/6694.

[8] Nigel Rambhujun, Muhammad Saad Salman, Ting Wang, Chulaluck Pratthana, Prabal Sapkota, Mehdi Costalin, Qiwen Lai, and Kondo-Francois Aguey-Zinsou. Renewable hydrogen for the chemical industry. *MRS Energy & Sustainability*, 7(1), 7 2020. doi: 10.1557/mre.2020.33. URL https://www.cambridge.org/core/journals/mrs-energy-and-sustainability/article/renewable-hydrogen-for-the-chemical-industry/83770CB2B5FC671F1F069A8CEB13E219.

[9] Elena Rozzi, Francesco Demetrio Minuto, Andrea Lanzini, and Pierluigi Leone. Green Synthetic Fuels: Renewable Routes for the Conversion of Non-Fossil Feedstocks into Gaseous Fuels and Their End Uses. *Energies*, 13(2):420, 1 2020. doi: 10.3390/en13020420. URL https://www.mdpi.com/1996-1073/13/2/420.

[10] Manish Kumar Singla, Parag Nijhawan, and Amandeep Singh Oberoi. Hydrogen fuel and fuel cell technology for cleaner future: a review. *Environmental Science and Pollution Research*, 28(13):15607–15626, 2 2021. doi: 10.1007/s11356-020-12231-8. URL https://doi.org/10.1007/s11356-020-12231-8.

[11] M.A. Aminudin, S.K. Kamarudin, B.H. Lim, E.H. Majilan, Masdar, and N. Shaari. An overview: Current progress on hydrogen fuel cell vehicles. *International Journal of Hydrogen Energy*, 48(11):4371–4388, 2 2023. doi: 10.1016/j.ijhydene.2022.10.156. URL https://www.sciencedirect.com/science/article/pii/S0360319922048534.

[12] Meiling Yue, H. Lambert, Elodie Pahon, Robin Roche, Samir Jemeï, and Daniel Hissel. Hydrogen energy systems: A critical review of technologies, applications, trends and challenges. *Renewable & Sustainable Energy Reviews*, 146:111180, 8 2021. doi: 10.1016/j.rser.2021.111180. URL https://doi.org/10.1016/j.rser.2021.111180.

[13] NWP. Hydrogen Roadmap for the Netherlands, 1 2021. URL https://nationaalwaterstofprogramma.nl/PageByID.aspx?sectionID=238846&contentPageID=2379389.

[14] A Wang, K van der Leun, D Peters, and M Buseman. European Hydrogen Backbone - How a dedicated hydrogen infrastructure can be created, 7 2020. URL https://ehb.eu/files/downloads/2020_European-Hydrogen-Backbone_Report.pdf.

[15] Gasunie. Hydrogen network netherlands. https://www.gasunie.nl/en/projects/hydrogen-network-netherlands, n.d. Accessed: 2024-04-14.

[16] G Tezel and R Hensgens. HyWay 27: hydrogen transmission using the existing natural gas grid?, 6 2021. URL https://www.hyway27.nl/en/latest-news/hyway-27-realisation-of-a-national-hydrogen-network.

[17] Reuters. Dutch limit groningen gas production despite energy crisis, 2023. URL https://www.reuters.com/business/energy/dutch-limit-groningen-gas-production-28-bcm-20222023-2022-09-26/.

[18] Matjaž Matošec. Repurposing gas transmission pipelines for hydrogen, 12 2023. URL https://hydrogentechworld.com/repurposing-gas-transmission-pipelines-for-hydrogen#:~:text=Repurposing%20natural%20gas%20infrastructure%20to,at%20typical%20transmission%20pipeline%20conditions.

[19] Karan Sotoodeh. Chapter 13 - piping and valve corrosion study. In Karan Sotoodeh, editor, *A Practical Guide to Piping and Valves for the Oil and Gas Industry*, pages 585–627. Gulf Professional Publishing, 2021. ISBN 978-0-12-823796-0. doi: https://doi.org/10.1016/B978-0-12-823796-0.00009-X. URL https://www.sciencedirect.com/science/article/pii/B978012823796000009X.

[20] Hongwei Zhang, Jie Zhao, Jingfa Li, Bo Yu, Jialong Wang, Ran Lyu, and Qian Xi. Research progress on corrosion and hydrogen embrittlement in hydrogen–natural gas pipeline transportation. *Natural Gas Industry*, 43:126–138, 12 2023. ISSN 10000976. doi: 10.3787/J.ISSN.1000-0976.2023.06.013.

[21] Paul Martin, Ilissa B. Ocko, Sofia Esquivel-Elizondo, Roland Kupers, David Cebon, Tom Baxter, and Steven P. Hamburg. A review of challenges with using the natural gas system for hydrogen. *Energy Science & Engineering*, 8 2024. doi: 10.1002/ese3.1861. URL `https://doi.org/10.1002/ese3.1861`.

[22] Gasunie. Gegevens hoofdgasnet in Nederland en veiligheidsprocedures, n.d. URL `https://www.energiebufferzuidwending.nl/bibliotheek/$421/$462`.

[23] Wenkang Zhang and Guanghui Zhao. Leakage and diffusion characteristics of underground hydrogen pipeline. *Petroleum*, 6 2023. ISSN 2405-6561. doi: 10.1016/J.PETLM.2023.06.002.

[24] W. Huinen. Onderzoek technische aspecten van waterstof in bestaande buisleidingen t.b.b. de energietransitie. Technical Report 53052.01-1917001, Bilfinger Tebodin, 11 2019. URL `https://open.overheid.nl/documenten/ronl-b50579b2-0461-4d88-98e5-9351a53e3692/pdf`.

[25] DINOloket. Ondergrondmodellen kaart. `https://www.dinoloket.nl/ondergrondmodellen/kaart`, n.d. Accessed: 2024-05-10.

[26] Ying Teng, Yongfeng Xu, Xiaomi Wang, and Peter Christie. Function of biohydrogen metabolism and related microbial communities in environmental bioremediation. *Frontiers in Microbiology*, 10:106, 2019. doi: 10.3389/fmicb.2019.00106.

[27] Anuj Chaudhary, Parul Chaudhary, Sami Abou Fayssal, Shivani Singh, Durges Kumar Jaiswal, Vishal Tripathi, and J. Kumar. *Exploring Beneficial Microbes and Their Multifaceted Applications: An Overview*. Microbial Inoculants, 2024. doi: 10.1007/978-981-97-0633-4_1.

[28] Oliver Schmidt, Linda Hink, Marcus A Horn, and Harold L Drake. Peat: home to novel syntrophic species that feed acetate- and hydrogen-scavenging methanogens. *The ISME Journal*, 10(8):1954–1966, 1 2016. doi: 10.1038/ismej.2015.256. URL `https://doi.org/10.1038/ismej.2015.256`.

[29] Xinyun Fan, Xuemeng Zhang, Guohua Zhao, Xin Zhang, Lei Dong, and Yinguang Chen. Aerobic hydrogen-oxidizing bacteria in soil: from cells to ecosystems. *Reviews in Environmental Science and Bio/Technology*, 21:877–04, 2022. doi: 10.1007/s11157-022-09633-0.

[30] Simon P. Gregory, Megan J. Barnett, Lorraine P. Field, and Antoni E. Milodowski. Subsurface microbial hydrogen cycling: Natural occurrence and implications for industry. *Subsurface Geomicrobiology*, 7(2):53, 2019. doi: 10.3390/microorganisms7020053.

[31] Sarah Piché-Choquette and PHilippe Constant. Molecular hydrogen, a neglected key driver of soil biogeochemical processes. *Applied and Environmental Microbiology*, 85(6), 2019. doi: 10.1128/aem.02418-18.

[32] Yufeng Jiang, Baogang Zhang, Chao He, Jiaxin Shi, Alistair G.L. Borthwick, and Xueyang Huang. Synchronous microbial vanadium (V) reduction and denitrification in groundwater using hydrogen as the sole electron donor. *Water Research*, 141:289–296, 9 2018. doi: 10.1016/j.watres.2018.05.033. URL https://www.sciencedirect.com/science/article/abs/pii/S0043135418304056.

[33] Maria Sand, Ragnhild Bieltvedt Skeie, Marit Sandstad, Srinath Krishnan, Gunnar Myhre, Hannah Bryant, Richard Derwent, Didier Hauglustaine, Fabien Paulot, Michael Prather, and David Stevenson. A multi-model assessment of the global warming potential of hydrogen. *Communications Earth & Environment 2023 4:1*, 4:1–12, 6 2023. ISSN 2662-4435. doi: 10.1038/s43247-023-00857-8. URL https://www.nature.com/articles/s43247-023-00857-8.

[34] Sandhiya Lakshmanan and Madhulika Bhati. Unravelling the atmospheric and climate implications of hydrogen leakage. *International Journal of Hydrogen Energy*, 53:807–815, 1 2024. ISSN 0360-3199. doi: 10.1016/J.IJHYDENE.2023.12.010.

[35] Katja Riedel, Keith Lassey, and NIWA. Detergent of the Atmosphere. Technical Report 1, NIWA, 2008. URL https://niwa.co.nz/sites/default/files/import/attachments/detergent.pdf.

[36] Xuexi Tie, C.Y.J. Kao, and E. J. Mroz. Net yield of OH, CO, and O3 from the oxidation of atmospheric methane. *Atmospheric Environment. Part A. General Topics*, 26(1):125–136, 1 1992. doi: 10.1016/0960-1686(92)90265-m. URL https://www.sciencedirect.com/science/article/pii/096016869290265M.

[37] Edward Topp and E. Pattey. Soils as sources and sinks for atmospheric methane. *Canadian Journal of Soil Science*, 77(2):167–177, 5 1997. doi: 10.4141/s96-107. URL https://doi.org/10.4141/s96-107.

[38] R.G. Derwent, William Collins, C. E. Johnson, and David S. Stevenson. Transient Behaviour of Tropospheric Ozone Precursors in a Global 3-D CTM and Their Indirect Greenhouse Effects. *Climatic Change*, 49(4):463–487, 1 2001. doi: 10.1023/a:1010648913655. URL https://doi.org/10.1023/a:1010648913655.

[39] Richard G. Derwent, David S. Stevenson, Steven R. Utembe, Michael E. Jenkin, Anwar H. Khan, and Dudley E. Shallcross. Global modelling studies of hydrogen and its isotopomers using stochem-cri: Likely radiative forcing consequences of a future hydrogen economy. *International Journal of Hydrogen Energy*, 45:9211–9221, 3 2020. ISSN 0360-3199. doi: 10.1016/J.IJHYDENE.2020.01.125.

[40] Martin Schultz, Thomas Diehl, Guy Brasseur, and Werner Zittel. Air pollution and Climate-Forcing impacts of a global hydrogen economy. *Science*, 302(5645):

624–627, 10 2003. doi: 10.1126/science.1089527. URL https://pubmed.ncbi.nlm.nih.gov/14576429/.

[41] N. J. Warwick, Slimane Bekki, E. G. Nisbet, and J. A. Pyle. Impact of a hydrogen economy on the stratosphere and troposphere studied in a 2-D model. *Geophysical Research Letters*, 31(5), 3 2004. doi: 10.1029/2003gl019224. URL https://doi.org/10.1029/2003gl019224.

[42] Robert A. Field and Richard G. Derwent. Global warming consequences of replacing natural gas with hydrogen in the domestic energy sectors of future low-carbon economies in the United Kingdom and the United States of America. *International Journal of Hydrogen Energy*, 46(58):30190–30203, 8 2021. doi: 10.1016/j.ijhydene.2021.06.120. URL https://doi.org/10.1016/j.ijhydene.2021.06.120.

[43] Alexander T. Archibald, J. L. Neu, Yasin Elshorbany, O. R. Cooper, Paul Young, Hideharu Akiyoshi, R. A. Cox, Mhairi Coyle, Richard G. Derwent, Makoto Deushi, Angelo Finco, G. J. Frost, Ian E. Galbally, Giacomo Gerosa, Claire Granier, Paul D. Griffiths, Ryan Hossaini, Lu Hu, Patrick Jöckel, B. Josse, Meiyun Lin, Mariano Mertens, Olaf Morgenstern, Manish Naja, Vaishali Naik, S. J. Oltmans, David A. Plummer, Laura E. Revell, Alfonso Saiz-Lopez, Pallavi Saxena, Youngsub Matthew Shin, Imran Shahid, Dudley E. Shallcross, Simone Tilmes, Thomas Trickl, Timothy J. Wallington, T. Wang, H. M. Worden, and Guang Zeng. Tropospheric Ozone Assessment Report. *Elementa*, 8(1), 1 2020. doi: 10.1525/elementa.2020.034. URL https://online.ucpress.edu/elementa/article/8/1/034/115205/Tropospheric-Ozone-Assessment-ReportA-critical.

[44] Ilissa B. Ocko and Steven P. Hamburg. Climate consequences of hydrogen emissions. *Atmospheric Chemistry and Physics*, 22(14):9349–9368, 7 2022. doi: 10.5194/acp-22-9349-2022. URL https://doi.org/10.5194/acp-22-9349-2022.

[45] J.B.R. Matthews, V. Möller, R. van Diemen, J.S. Fuglestvedt, V. Masson-Delmotte, C. Méndez, S. Semenov, and A. Reisinger. Annex vii: Glossary. In V. Masson-Delmotte, P. Zhai, A. Pirani, S.L. Connors, C. Péan, S. Berger, N. Caud, Y. Chen, L. Goldfarb, M.I. Gomis, M. Huang, K. Leitzell, E. Lonnoy, J.B.R. Matthews, T.K. Maycock, T. Waterfield, O. Yelekçi, R. Yu, and B. Zhou, editors, *Climate Change 2021: The Physical Science Basis. Contribution of Working Group I to the Sixth Assessment Report of the Intergovernmental Panel on Climate Change*, pages 2215–2256. Cambridge University Press, Cambridge, United Kingdom and New York, NY, USA, 2021. doi: 10.1017/9781009157896.022.

[46] Dick Derwent. HYDROGEN FOR HEATING: ATMOSPHERIC IMPACTS A: Literature review. Technical Report BEIS research paper Number 2018: no. 21, Department for Business, Energy & Industrial Strategy, 2018. URL https://assets.publishing.service.gov.uk/government/uploads/system/uploads/attachment_data/file/760538/Hydrogen_atmospheric_impact_report.pdf.

[47] Hoesung Lee, Katherine Calvin, Dipak Dasgupta, Gerhard Krinner, Aditi Mukherji, Peter Thorne, Christopher Trisos, José Romero, Paulina Aldunce, Ko Barrett, Gabriel Blanco, William W. L. Cheung, Sarah L. Connors, Fatima Denton, Aïda Diongue-Niang, David Dodman, Matthias Garschagen, Oliver Geden, Bronwyn Hayward, Christopher Jones, Frank Jotzo, Thelma Krug, Rodel Lasco, June-Yi Lee, Valérie Masson-Delmotte, Malte Meinshausen, Katja Mintenbeck, Abdalah Mokssit, Friederike E. L. Otto, Minal Pathak, Anna Pirani, Elvira Poloczanska, Hans-Otto Pörtner, Aromar Revi, Debra C. Roberts, Joyashree Roy, Alex C. Ruane, Jim Skea, Priyadarshi R. Shukla, Raphael Slade, Aimée Slangen, Youba Sokona, Anna A. Sörensson, Melinda Tignor, Detlef van Vuuren, Yi-Ming Wei, Harald Winkler, Panmao Zhai, and Zinta Zommers. Climate Change 2023: Synthesis report. Technical report, Intergovernmental Panel on Climate Change, 2023. URL `https://www.ipcc.ch/report/ar6/syr/downloads/report/IPCC_AR6_SYR_FullVolume.pdf`.

[48] Fabien Paulot, David Paynter, Vaishali Naik, Sergey Malyshev, Raymond Menzel, and Larry W. Horowitz. Global modeling of hydrogen using GFDL-AM4.1: Sensitivity of soil removal and radiative forcing. *International Journal of Hydrogen Energy*, 46(24):13446–13460, 4 2021. doi: 10.1016/j.ijhydene.2021.01.088. URL `https://doi.org/10.1016/j.ijhydene.2021.01.088`.

[49] Jianwei Li, Jie Liu, Tianci Wang, Weitao Zou, Qingqing Yang, and Jun Shen. Analysis of the evolution characteristics of hydrogen leakage and diffusion in a temperature stratified environment. *Energy*, 293:130598, 4 2024. ISSN 0360-5442. doi: 10.1016/J.ENERGY.2024.130598. URL `https://linkinghub.elsevier.com/retrieve/pii/S0360544224003700`.

[50] O.C. Zienkiewicz and R.L. Taylor. *The Finite Element Method*. McGraw-Hill, 1977.

[51] COMSOL. *CFD Module User's Guide*. COMSOL Multiphysics, 2019. URL `https://www.comsol.com`. Version: COMSOL 5.5.

[52] Frank M. White. *Fluid Mechanics*. McGraw-Hill, 6th edition, 2006.

[53] Stephen B. Pope. *Turbulent Flows*. Cambridge University Press, 2000. doi: 10.1017/cbo9780511840531.

[54] Dale C. Wilcox. *Turbulence Modeling for CFD*. DCW Industries, 3rd edition, 2006.

[55] Donald A. Nield and Adrian Bejan. *Convection in Porous Media*. Springer Science & Business Media, 4th edition, 2012.

[56] Ioan Pop and Derek B. Ingham. *Transport Phenomena in Porous Media II*. Pergamon, 2002. doi: https://doi.org/10.1016/B978-0-08-043965-5.X5000-4.

[57] Jacob Bear. *Dynamics of Fluids in Porous Media*. Courier Corporation, 1988.

[58] Stephen Whitaker. The forchheimer equation: A theoretical development. *Transport in Porous Media*, 25(1):27–61, 1996. doi: https://doi.org/10.1007/BF00141261.

[59] Civil Lead. Density of Cement, Sand and Aggregate, Bulk Density of Aggregate - Civil Lead, 6 2022. URL https://www.civillead.com/density-of-cement-sand-and-aggregate/.

[60] Ubani Obinna. Soil Classification and Typical Engineering Properties of Soils - Structville, 1 2024. URL https://structville.com/soil-classification-and-engineering-properties.

[61] Donald A. Nield and Adrian Bejan. *Convection in Porous Media*. Springer International Publishing, Cham, 5 edition, 2017. ISBN 978-3-319-49562-0. doi: 10.1007/978-3-319-49562-0. URL https://link.springer.com/book/10.1007/978-3-319-49562-0.

[62] Alessandro Lenci, Farhad Zeighami, and Vittorio Di Federico. Effective forchheimer coefficient for layered porous media. *Transport in Porous Media*, 144(2):459–480, 2022. doi: 10.1007/s11242-022-01815-2. URL https://link.springer.com/article/10.1007/s11242-022-01815-2.

[63] A. E. Yekta, J.-c. Manceau, S. Gaboreau, M. Pichavant, and P. Audigane. Determination of Hydrogen–Water relative permeability and capillary pressure in sandstone: application to underground hydrogen injection in sedimentary formations. *Transport in porous media*, 122(2):333–356, 1 2018. doi: 10.1007/s11242-018-1004-7. URL https://doi.org/10.1007/s11242-018-1004-7.

[64] Cunjin Lu, Longfei Li, Jinpeng Xu, Hui Zhao, and Mingyue Chen. Research on the Critical Value of Sand Permeability Particle Size and Its Permeability Law after Mixing. *Water*, 16(3):393, 1 2024. doi: 10.3390/w16030393. URL https://www.mdpi.com/2073-4441/16/3/393.

[65] O.R. Jones and W.C. McCabe. Permeability of soil and rock for gas and liquid migration: The effect of soil composition on gas permeability. *Journal of Geotechnical and Geoenvironmental Engineering*, 125(2):101–108, 1999. doi: 10.1061/(ASCE)1090-0241(1999)125:2(101).

[66] A.A. Malakhov, A.V. Avdeenkov, M.H. Du Toit, and D.G. Bessarabov. CFD simulation and experimental study of a hydrogen leak in a semi-closed space with the purpose of risk mitigation. *International Journal of Hydrogen Energy*, 45 (15):9231–9240, 3 2020. doi: 10.1016/j.ijhydene.2020.01.035. URL https://www.sciencedirect.com/science/article/pii/S0360319920300999.

[67] K. Hartmann, C. Correa-Jullian, J. Thorson, K. Groth, Center for Energy Conversion, Storage Systems, Center for Risk, and Reliability. HYDROGEN COMPONENT LEAK RATE QUANTIFICATION FOR SYSTEM RISK AND RELIABILITY ASSESSMENT THROUGH QRA AND PHM FRAMEWORKS. Technical report, HySafe, 2021. URL https://hysafe.info/uploads/papers/2021/157.pdf#:~:text=URL%3A%20https%3A%2F%2Fhysafe.info%2Fuploads%2Fpapers%2F2021%2F157.pdf%0AVisible%3A%200%25%20.

[68] Jorgen Depken, Alexander Dyck, Lukas Roß, and Sören Ehlers. Safety considerations of hydrogen application in shipping in comparison to LNG. *Energies*, 15(9):3250, 4 2022. doi: 10.3390/en15093250. URL https://www.mdpi.com/1996-1073/15/9/3250.

[69] European Gas Pipeline Incident Data Group (EGIG). Gas pipeline incidents: 11th report of the european gas pipeline incident data group (period 1970 – 2019). Technical report, EGIG, Groningen, Netherlands, December 2020. URL https://www.egig.eu/. Doc. number VA 20.0432.

[70] Government of the Netherlands. Government strategy on hydrogen, 2020. URL https://www.government.nl/documents/publications/2020/04/06/government-strategy-on-hydrogen.

[71] Barthold Schroot. The netherlands: a blue hydrogen economy now will ease a transition to green, 2021. URL https://energypost.eu/the-netherlands-a-blue-hydrogen-economy-now-will-ease-a-transition-to-green/.

[72] International Energy Agency. Global hydrogen review 2022, 2022. URL https://iea.blob.core.windows.net/assets/c5bc75b1-9e4d-460d-9056-6e8e626a11c4/GlobalHydrogenReview2022.pdf.

[73] International Energy Agency. The netherlands - energy mix, 2024. URL https://www.iea.org/countries/the-netherlands/energy-mix.

[74] Richard B. Kuprewicz. Safety of hydrogen transportation by gas pipelines, November 28 2022. URL https://pstrust.org/wp-content/uploads/2022/11/11-28-22-Final-Accufacts-Hydrogen-Pipeline-Report.pdf. Prepared for the Pipeline Safety Trust.

[75] Naga Venkata Saidileep Korlapati, Faisal Khan, Quddus Noor, Saadat Mirza, and Sreeram Vaddiraju. Review and analysis of pipeline leak detection methods. *Journal of Pipeline Science and Engineering*, 2(4):100074, 12 2022. doi: 10.1016/j.jpse.2022.100074. URL https://www.sciencedirect.com/science/article/pii/S2667143322000464.

[76] Qingqing Xu, Laibin Zhang, and Wei Liang. Acoustic detection technology for gas pipeline leakage. *Process Safety and Environmental Protection*, 91(4):253–261, 7 2013. doi: 10.1016/j.psep.2012.05.012. URL https://www.sciencedirect.com/science/article/pii/S0957582012000572.

[77] Jinqiu Hu, Laibin Zhang, and Wei Liang. Detection of small leakage from long transportation pipeline with complex noise. *Journal of Loss Prevention in the Process Industries*, 24(4):449–457, 7 2011. doi: 10.1016/j.jlp.2011.04.003. URL https://doi.org/10.1016/j.jlp.2011.04.003.

[78] Lingya Meng, Li Yuxing, Wang Wuchang, and Fu Juntao. Experimental study on leak detection and location for gas pipeline based on acoustic method. *Journal of Loss Prevention in the Process Industries*, 25(1):90–102, 1 2012. doi: 10.1016/j.jlp.2011.07.001. URL https://www.sciencedirect.com/science/article/pii/S0950423011001112.

[79] Zhongyu Hu, Salman Tariq, and Tarek Zayed. A comprehensive review of acoustic based leak localization method in pressurized pipelines. *Mechanical Systems and Signal Processing*, 161:107994, 12 2021. doi: 10.1016/j.ymssp.2021.107994. URL https://www.sciencedirect.com/science/article/pii/S0888327021003897.

[80] R. Ramadevi, J. Jaiganesh, and N. R. Krishnamoorthy. *Leak Detection Methods—A Technical Review*. ICCCE 2018, 9 2018. doi: 10.1007/978-981-13-0212-1\{_}14. URL https://doi.org/10.1007/978-981-13-0212-1_14.

[81] J.M. Muggleton, R. Hunt, E. Rustighi, G. Lees, and A. Pearce. Gas pipeline leak noise measurements using optical fibre distributed acoustic sensing. *Journal of Natural Gas Science and Engineering*, 78:103293, 6 2020. doi: 10.1016/j.jngse.2020.103293. URL https://www.sciencedirect.com/science/article/pii/S1875510020301475.

[82] Thomas Allsop and Ronald Neal. A Review: Application and Implementation of Optic Fibre Sensors for Gas Detection. *Sensors*, 21(20):6755, 10 2021. doi: 10.3390/s21206755. URL https://www.mdpi.com/1424-8220/21/20/6755.

[83] Mahmoud Meribout, Lyes Khezzar, Abdelwahid Azzi, and Nabil Ghendour. Leak detection systems in oil and gas fields: Present trends and future prospects. *Flow Measurement and Instrumentation*, 75:101772, 10 2020. doi: 10.1016/j.flowmeasinst.2020.101772. URL https://www.sciencedirect.com/science/article/pii/S0955598620301205.

[84] Afifi bin Md Akib, Nordin bin Saad, and Vijanth Asirvadam. Pressure point analysis for early detection system. In *2011 IEEE 7th International Colloquium on Signal Processing and its Applications*, pages 103–107, 2011. doi: 10.1109/CSPA.2011.5759852.

[85] Hongfang Lu, Tom Iseley, Saleh Behbahani, and Lingdi Fu. Leakage detection techniques for oil and gas pipelines: State-of-the-art. *Tunnelling and Underground Space Technology*, 98:103249, 4 2020. doi: 10.1016/j.tust.2019.103249. URL https://doi.org/10.1016/j.tust.2019.103249.

[86] Mutiu Adesina Adegboye, Wai-Keung Fung, and Aditya Karnik. Recent Advances in Pipeline Monitoring and Oil Leakage Detection Technologies: Principles and Approaches. *Sensors*, 19(11):2548, 6 2019. doi: 10.3390/s19112548. URL https://www.mdpi.com/1424-8220/19/11/2548.

[87] Norazlina Subani, Norsarahaida Amin, and Baba Galadima Agaie. Leak detection of non-isothermal transient flow of hydrogen-natural gas mixture. *Journal of Loss Prevention in the Process Industries*, 48:244–253, 7 2017. doi: 10.1016/j.jlp.2017.05.003. URL https://www.sciencedirect.com/science/article/pii/S0950423017304369.

[88] Jinhai Liu, Hanguang Su, Yanjuan Ma, Gang Wang, Yuan Wang, and Kun Zhang. Chaos characteristics and least squares support vector machines based online pipeline small leakages detection. *Chaos Solitons & Fractals*, 91:656–669, 10 2016. doi: 10.1016/j.chaos.2016.09.002. URL https://www.sciencedirect.com/science/article/pii/S0960077916302545.

[89] B.M.S. Arifin, Zukui Li, and Sirish L. Shah. Pipeline leak detection using particle filters. *IFAC-PapersOnLine*, 48(8):76–81, 1 2015. doi: 10.1016/j.ifacol.2015.08.160. URL https://www.sciencedirect.com/science/article/pii/S2405896315010277.

[90] Tarek R. Sheltami, Abubakar Bala, and Elhadi M. Shakshuki. Wireless sensor networks for leak detection in pipelines: a survey. *Journal of Ambient Intelligence and Humanized Computing*, 7(3):347–356, 3 2016. doi: 10.1007/s12652-016-0362-7. URL https://doi.org/10.1007/s12652-016-0362-7.

[91] Luca Surace, Massimiliano Sorrentino, and Fabio Capaldi. LDS - Leak Detection System at Trieste/Visco Pipeline. *Society of Petroleum Engineers*, 10 2019. doi: 10.2118/198168-ms. URL https://doi.org/10.2118/198168-ms.

[92] Wei Liang, Jian Kang, and Laibin Zhang. Leak detection for long transportation pipeline using a state coupling analysis of pump units. *Journal of Loss Prevention in the Process Industries*, 26(4):586–593, 7 2013. doi: 10.1016/j.jlp.2012.12.007. URL https://doi.org/10.1016/j.jlp.2012.12.007.

[93] Wenqing Lu, Wei Liang, Laibin Zhang, and Wei Liu. A novel noise reduction method applied in negative pressure wave for pipeline leakage localization. *Process Safety and Environmental Protection*, 104:142–149, 11 2016. doi: 10.1016/j.psep.2016.08.014. URL https://doi.org/10.1016/j.psep.2016.08.014.

[94] Kenya Fukushima, Reiko Maeshima, Akira Kinoshita, Hitoshi Shiraishi, and Ichiro Koshijima. Gas pipeline leak detection system using the online simulation method. *Computers & Chemical Engineering*, 24(2-7):453–456, 7 2000. doi: 10.1016/s0098-1354(00)00442-7. URL https://doi.org/10.1016/s0098-1354(00)00442-7.

[95] Morgan Henrie, Philip Carpenter, and R. Edward Nicholas. *Mass balance leak detection*. Elsevier, 1 2016. doi: 10.1016/b978-0-12-802240-5.00003-0. URL https://doi.org/10.1016/b978-0-12-802240-5.00003-0.

[96] JonathaN. Rougier. Probabilistic leak detection in pipelines using the mass imbalance approach. *Journal of Hydraulic Research*, 43(5):556–566, 9 2005. doi: 10.1080/00221680509500154. URL https://doi.org/10.1080/00221680509500154.

[97] Akhand Rai and Jong-Myon Kim. A novel pipeline leak detection approach independent of prior failure information. *Measurement*, 167:108284, 1 2021. doi: 10.1016/j.measurement.2020.108284. URL https://doi.org/10.1016/j.measurement.2020.108284.

[98] Michel Saade and Samir Mustapha. Assessment of the structural conditions in steel pipeline under various operational conditions – A machine learning approach. *Measurement*, 166:108262, 12 2020. doi: 10.1016/j.measurement.2020.108262. URL https://doi.org/10.1016/j.measurement.2020.108262.

[99] Jun Zhang. Designing a cost-effective and reliable pipeline leak-detection system. *Pipes and Pipelines International*, 42(1):20–26, 1 1997. URL https://www.scopus.com/record/display.uri?eid=2-s2.0-0030732783&origin=inward.

[100] Alireza Keramat, Xun Wang, Moez Louati, Silvia Meniconi, Bruno Brunone, and Mohamed S Ghidaoui. Objective functions for transient-based pipeline leakage detection in a noisy environment: least square and matched-filter. *Journal of Water Resources Planning and Management*, 145(10):04019042, 2019.

[101] Richard B. Kuprewicz. Observations on the Application of Smart Pigging on Transmission Pipelines. Technical report, Accufacts Inc., 9 2005. URL http://www.pstrust.org/.

[102] Jian Du and Jianqin Zheng. *Intelligent Leakage Detection for Pipelines*, pages 177–188. Springer Nature Singapore, Singapore, 2023. ISBN 978-981-19-9899-7. doi: 10.1007/978-981-19-9899-7_11. URL https://doi.org/10.1007/978-981-19-9899-7_11.

[103] Simin Wang, Huaiying Jiang, Bin Wang, Jiansen Du, Shang Wang, and Lei Qin. A Technique for Detecting Hydrogen and Methane Using Refractive Index Sensitivity. *Process Safety and Environmental Protection*, 5 2024. doi: 10.1016/j.psep.2024.05.131. URL https://www.sciencedirect.com/science/article/pii/S0957582024006530.

[104] Solomon Adenubi, Dulu Appah, Emeka Okafor, and Victor Aimikhe. A Review of Leak Detection Systems for Natural Gas Pipelines and Facilities. *Deleted Journal*, 4 2023. doi: 10.7176/jetp/13-2-02. URL https://doi.org/10.7176/jetp/13-2-02.

[105] Arvind P Ravikumar, Daniel Roda-Stuart, Ryan Liu, Alexander Bradley, Joule Bergerson, Yuhao Nie, Siduo Zhang, Xiaotao Bi, and Adam R Brandt. Repeated leak detection and repair surveys reduce methane emissions over scale of years. *Environmental Research Letters*, 15(3):034029, 2 2020. doi: 10.1088/1748-9326/ab6ae1. URL https://doi.org/10.1088/1748-9326/ab6ae1.

[106] Point Safety. Hydrogen gas detectors - portable gas detectors, n.d. URL https://gasmonitor-point.co.uk/hydrogen-gas-detector.

[107] Norsk Analyse. Hy-alerta™ 500 handheld hydrogen leak detector, 2024. URL https://www.norskanalyse.com/produkt/hy-alerta-500-handheld-hydrogen-leak-detector/. Accessed: 2024-08-29.

[108] Joel H. Ferziger and Milovan Perić. *Computational Methods for Fluid Dynamics*. Springer Berlin, Heidelberg, 1 2002. doi: 10.1007/978-3-642-56026-2. URL https://doi.org/10.1007/978-3-642-56026-2.

[109] Ronald J. Chila and Deborah A. Kaminski. Grid independence via automated unstructured adaptation. *Journal of Fluids Engineering*, 130(12), 10 2008. doi: 10.1115/1.3001099. URL https://asmedigitalcollection.asme.org/fluidsengineering/article-abstract/130/12/121403/439383/Grid-Independence-Via-Automated-Unstructured?redirectedFrom=fulltext.

[110] D. Green C. Brown. Impact of soil permeability on pipeline leakage: A comparative study between clay and sand. *Environmental Engineering Science*, 38(7):912–920, 2021. doi: 10.1089/ees.2020.0175.

[111] Pedro Barbosa. Achieving accurate leak detection in hydrogen pipelines. *World Pipelines*, 2022. URL https://www.worldpipelines.com/special-reports/01112022/achieving-accurate-leak-detection-in-hydrogen-pipelines/.

[112] Muhammad Farooq Siddique, Zahoor Ahmad, Niamat Ullah, Saif Ullah, and Jong-Myon Kim. Pipeline leak detection: A comprehensive deep learning model using cwt image analysis and an optimized dbn-ga-lssvm framework. *Sensors*, 24(12): 4009, 2024. doi: 10.3390/s24124009.

[113] B. Johnson A. Smith. Comparison of permeability and soil properties between sand and clay. *Journal of Geotechnical Engineering*, 45(3):678–687, 2019. doi: 10.1016/j.geotech.2019.06.003.

[114] M. Yang, J. Lee, and S. Park. Effect of defect size and location on gas pipeline leakage and failure: A computational fluid dynamics study. *Journal of Pressure Vessel Technology*, 136(6):061702, 2014. doi: 10.1115/1.4028530.

[115] N.V. Nederlandse Gasunie. Gasunie jaarverslag 2023, 2023. URL https://www.publicatiesgasunie.nl/jaarverslag-2023. Accessed: August 26, 2024.

A Appendix

Additional Governing Equations and Constants

The following constants and auxiliary relations are used in the κ-ω Low Reynolds number model:

$$\alpha = \frac{13}{25}, \quad \beta = \beta_0 f_\beta, \quad \beta^* = \beta_0^* f_\beta^*, \quad \sigma = \frac{1}{2}, \quad \sigma^* = \frac{1}{2} \tag{A.1}$$

$$\beta_0 = \frac{13}{125}, \quad f_\beta = \frac{1+70\chi_\omega}{1+80\chi_\omega}, \quad \chi_\omega = \left| \frac{\Omega_{ij}\Omega_{jk}S_{ki}}{(\beta_0^*\omega)^3} \right| \tag{A.2}$$

$$\beta_0^* = \frac{9}{100}, \quad f_\beta^* = \begin{cases} 1 & \chi_k \leq 0 \\ \frac{1+680\chi_k^2}{1+400\chi_k^2} & \chi_k > 0 \end{cases}, \quad \chi_k = \frac{1}{\omega^3}(\nabla \cdot \nabla\omega) \tag{A.3}$$

where Ω_{ij} is the mean rotation-rate tensor:

$$\Omega_{ij} = \frac{1}{2}\left(\frac{\partial \bar{u}_i}{\partial x_j} - \frac{\partial \bar{u}_j}{\partial x_i}\right) \tag{A.4}$$

and S_{ij} is the mean strain-rate tensor:

$$S_{ij} = \frac{1}{2}\left(\frac{\partial \bar{u}_i}{\partial x_j} + \frac{\partial \bar{u}_j}{\partial x_i}\right) \tag{A.5}$$

The production term P_k is given by equation 3.7. The following auxiliary relations for the dissipation, ϵ, and the turbulent mixing length, l_*, are also used:

$$\epsilon = \beta^*\omega k, \quad l_{\text{mix}} = \frac{\sqrt{k}}{\omega} \tag{A.6}$$

Variable Descriptions

- $\alpha, \beta, \beta^*, \sigma, \sigma^*$: Model constants.
- β_0, β_0^*: Base values for model constants.
- f_β, f_β^*: Functions modifying the base model constants.
- χ_ω, χ_k: Dimensionless variables used in the model.
- Ω_{ij}: Mean rotation-rate tensor, describing the rotation rate of the flow.
- S_{ij}: Mean strain-rate tensor, describing the deformation rate of the flow.

- ϵ: Turbulent dissipation rate.
- l_{mix}: Turbulent mixing length, indicating the scale of turbulent eddies.
- $\bar{u}_i$: Components of the mean velocity vector.
- x_i, x_j: Spatial coordinates.

Sand vs Clay all scenarios

Figures A.1 and A.2 show the leakage rate and the horizontal dispersion range in sand and clay for each scenario and leak size.

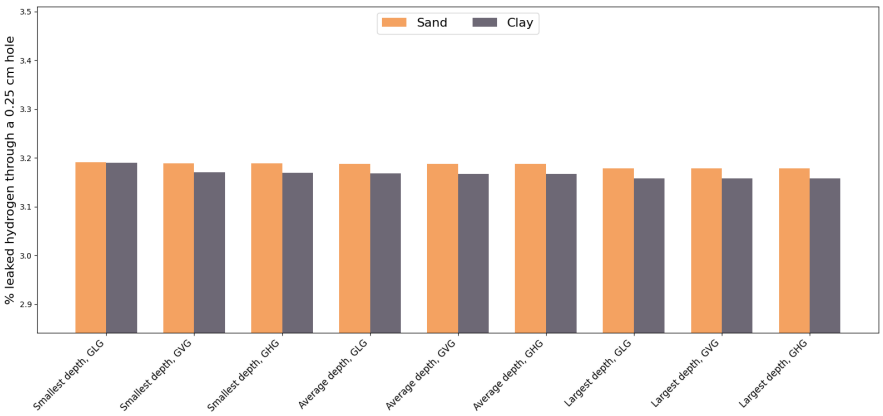

(a) Hole size 0.25 cm

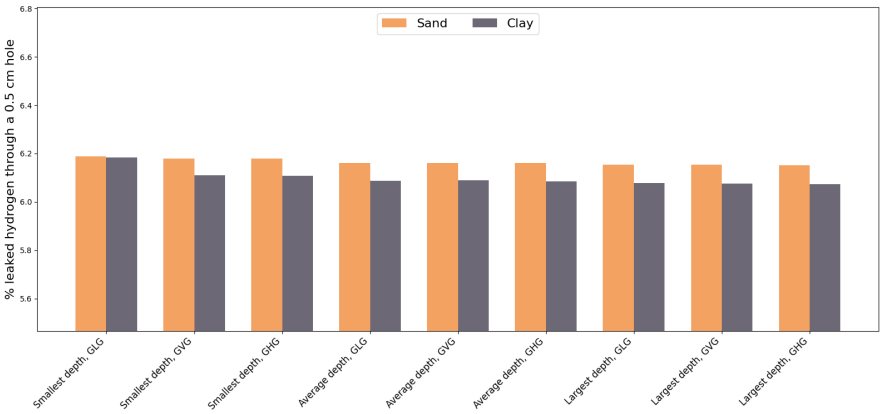

(b) Hole size 0.5 cm

Figure A.1: The percentage of hydrogen leaked in sand and clay for different depths of pipes and groundwater levels. (continued)

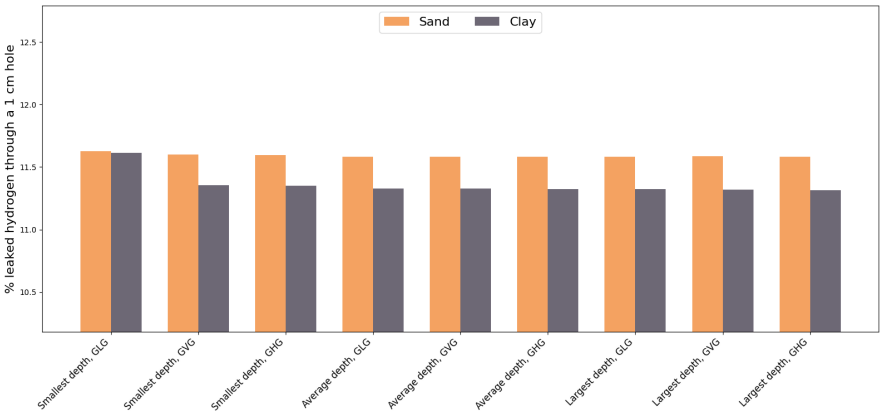

(c) Hole size 1 cm

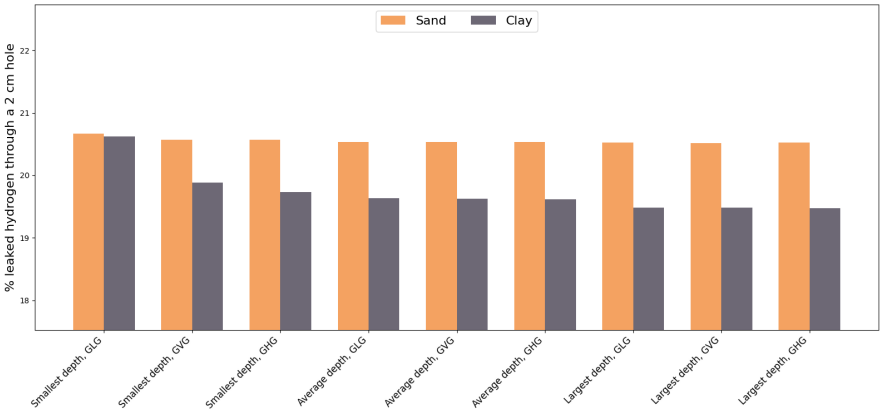

(d) Hole size 2 cm

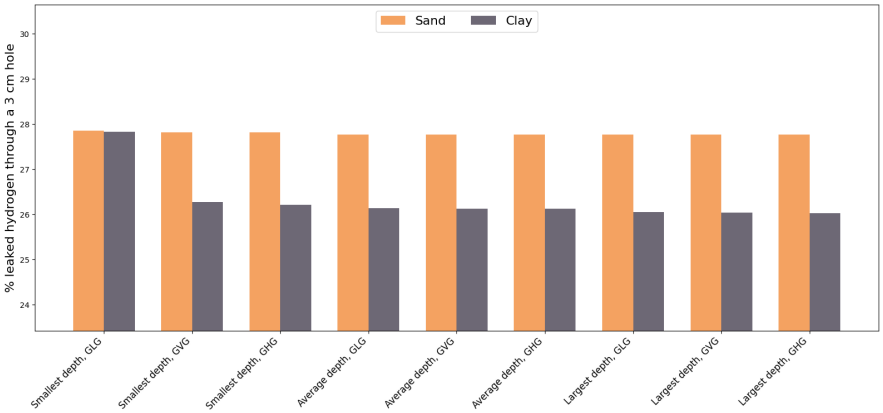

(e) Hole size 3 cm

Figure A.1: The percentage of hydrogen leaked in sand and clay for different depths of pipes and groundwater levels.

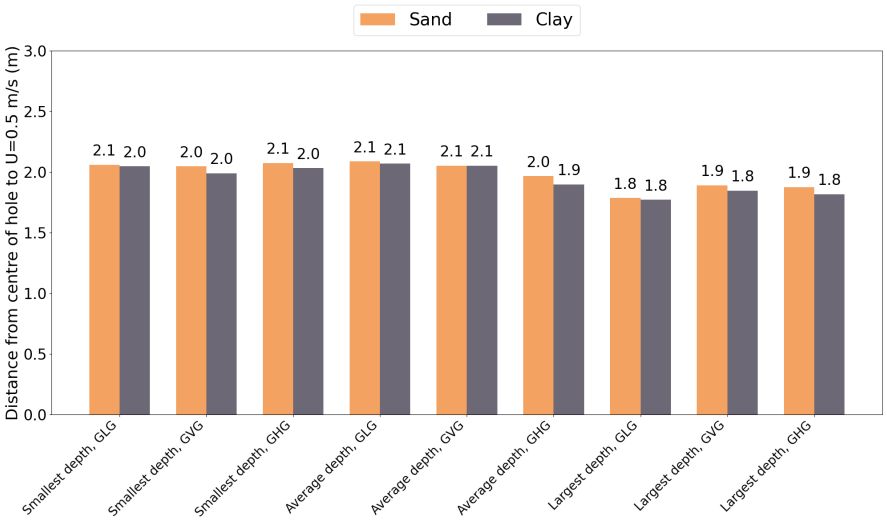

(a) Hole size 0.25 cm

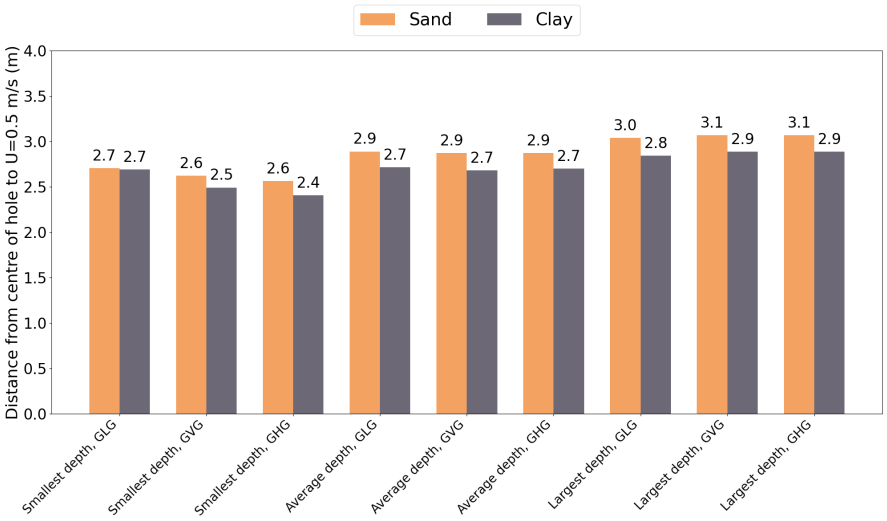

(b) Hole size 0.5 cm

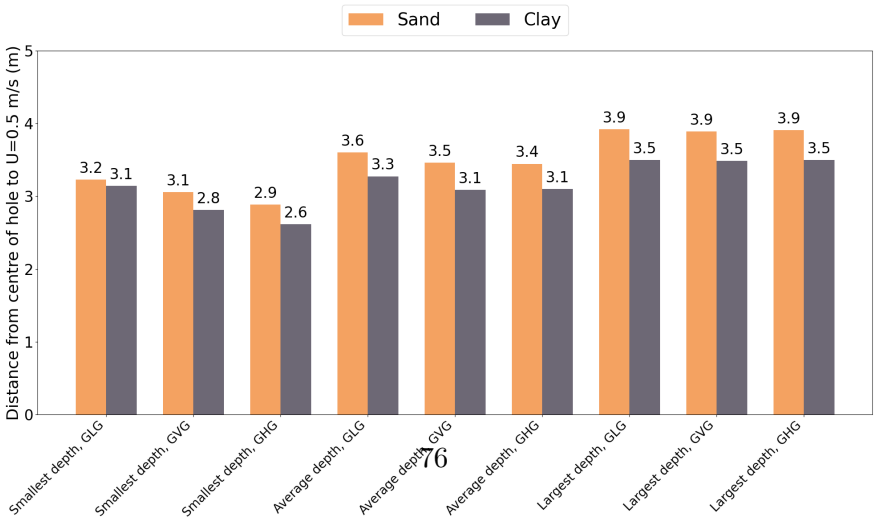

(c) Hole size 1 cm

Figure A.2: The horizontal dispersion of hydrogen measured from the center of the hole to the point where the velocity reaches 0.5 m/s (continued).

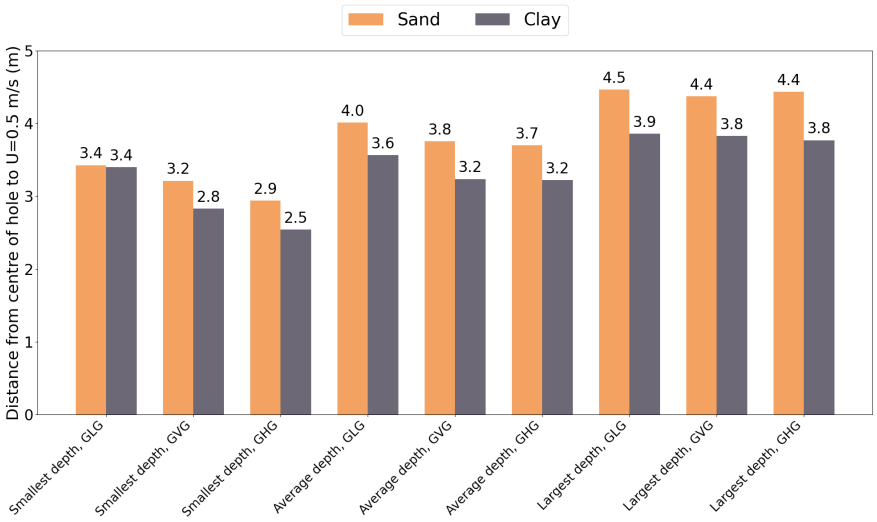

(d) Hole size 2 cm

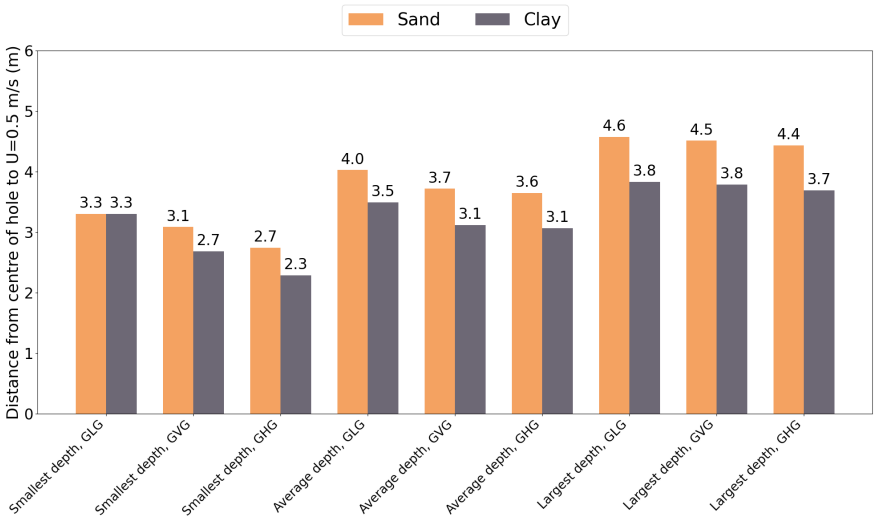

(e) Hole size 3 cm

Figure A.2: The horizontal dispersion of hydrogen measured from the center of the hole to the point where the velocity reaches 0.5 m/s (conclusion).